國立臺灣大學醫學院臨床醫學研究所

碩士論文

Graduate Institute of Clinical Medicine

College of Medicine

National Taiwan University

Master's Thesis

原發性震顫患者接受磁振導航聚焦超音波丘腦燒灼術後之短期與長期腦部結構變化

Short- and Long-Term Structural Changes in Essential Tremor Following MRgFUS Thalamotomy

林昀

Yun Lin

指導教授：趙啟超博士

呂明桂博士

Advisors: Chih-Chao Chao, MD, Ph.D.

Ming-Kuei Lu, MD, Ph.D.

中華民國 114 年 7 月

July 2025

doi:10.6342/NTU202504209

致謝

過去的我對研究全無概念，十分感謝趙啟超老師、呂明桂老師的指導，讓我從頭開始學習，給予全然懞懂無知的我無盡的包容和耐心引導；謝謝君明學長在影像技術上的協助、不吝花時間陪我克服完全沒有頭緒的技術問題、並在必要時伸出援手。謝謝頌儒學長帶我入門學習使用 DSI studio，讓我在茫然無措的時候找到一個實際且可行的切入點，開始有信心和方向進行接下來的分析。謝謝李佳霙老師指點我如何使用統計方法克服病人收案過程的瑕疵，讓我對解決問題的方式更有確信，也在過程中認識到臨床研究材料條件難以合乎理想時，統計知識是重要的工具。感謝願意支持這項研究的對照組受試者們，也謝謝願意協助我在門診篩選合適參與者的師長和前輩、謝謝所有願意配合回院追蹤的病人，是你們讓這個研究有從動機發展出實質內容的機會。謝謝無條件支持我的家人，讓我在一連串新事物的試誤學習中能有奮鬥的底氣。有辦法得到一點點歸納分析的成果，實在離不開各種良善的機緣，在學習研究的過程中，能有任何進展都是得力於好多不同人的幫忙。

此外，也感謝蔡主任與所有在研究進行期間提供協助的相關人員，使本研究順利完成。不知不覺好不容易向前邁出了最小的一步，最後仍然希望大力感謝我的兩位指導老師，謝謝趙老師在從起點推進研究的過程中給我很多實質的建議和指導，沒有老師的指引，如何到達目的地應該一直都會非常抽象迷茫；謝謝呂老師願意支持我，讓這趟旅程得以成真。

doi:10.6342/NTU202504209

中文摘要

原發性顫抖(Essential tremor)是一種常見的神經科疾病，雖然對健康不致於造成重大危害，但卻足以造成日常生活相當具體的不便，在部分病人也連帶產生社交退縮等心理影響。目前對於原發性顫抖的治療分為藥物及手術兩種方式，藥物治療雖然簡便，但在不少病人身上卻難以達到理想的效果。磁振導航聚焦超音波丘腦燒灼術(MRgFUS thalamotomy)是一種非侵襲性的手術方式，藉由非侵入性的方式在丘腦精準地形成病灶以治療顫抖，目前已經是不少病人替代服藥的治療方式。

要了解原發性顫抖為何能從磁振導航聚焦超音波丘腦燒灼術獲得治療效益，牽涉到對於疾病生理的了解。本研究試圖透過原發性顫抖患者與對照組、原發性顫抖患者磁振導航聚焦超音波丘腦燒灼術術前與術後早期、術後晚期不同時間的比較，探討疾病本身以及聚焦超音波丘腦燒灼對於腦內結構的影響。我們發現原發性顫抖病人與對照組相比，其胼胝體的體積有所不同；另外，經手術治療後，發現病人胼胝體(corpus callosum)及小腦腳出現微結構以及巨觀的體積改變，暗示了疾病的改善伴隨了跨大腦半球訊息傳導的變化，也呼應了目前對於原發性顫抖是一種「神經網絡疾病」(network disease)的觀點。

本研究受限於樣本數及影像分析技術本身的限制，難以完全揭示原發性顫抖的病態生理以及接受丘腦燒灼術後腦部構造與功能的完整變化，尚待其他更完備之研究進行驗證。

關鍵字:原發性顫抖、核磁共振影像、擴散張量影像、像素型態測量學、Fahn-Tolosa-Marin 震顫評定量表

doi:10.6342/NTU202504209

Abstract

Essential tremor (ET) is a common neurological disorder. Although it does not pose a major threat to overall health, it can cause significant inconvenience in daily life and, in some patients, lead to psychological effects such as social withdrawal. Current treatment strategies for ET include both pharmacological and surgical approaches. While medications are convenient, they often fail to produce satisfactory results in many patients. Magnetic Resonance-guided Focused Ultrasound (MRgFUS) thalamotomy is a non-invasive surgical technique that precisely targets and ablates regions in the thalamus to alleviate tremor, and it has become an alternative treatment for patients who do not respond well to medication. Understanding why MRgFUS thalamotomy benefits patients with ET requires insight into the disease's underlying pathophysiology. This study compares ET patients with healthy controls, as well as pre- and post-operative imaging (early and late phases) of ET patients undergoing MRgFUS thalamotomy, to investigate the structural brain changes associated with both the disease itself and the surgical intervention. We found that compared to healthy controls, ET patients exhibited differences in the volume of the corpus callosum and cerebellar peduncles. Furthermore, both microstructural and macrostructural changes in the corpus callosum and cerebellar peduncles were observed following MRgFUS thalamotomy, suggesting that improvements in tremor may be accompanied by alterations in interhemispheric communication. These findings support the current view that ET may be a "network disease."

However, this study is limited by its small sample size and inherent constraints of neuroimaging techniques, and it may not fully capture the pathological mechanisms of ET or the comprehensive structural and functional changes following thalamotomy. Further

doi:10.6342/NTU202504209

studies with larger cohorts and advanced imaging methods are warranted to validate these findings.

Keywords: Essential tremor, magnetic resonance imaging, diffusion tensor imaging, voxel-based morphometry, Fahn-Tolosa-Marin Tremor Rating Scale

doi:10.6342/NTU202504209

目次

doi:10.6342/NTU202504209

doi:10.6342/NTU202504209

doi:10.6342/NTU202504209

doi:10.6342/NTU202504209

圖次

doi:10.6342/NTU202504209

表次

doi:10.6342/NTU202504209

doi:10.6342/NTU202504209

doi:10.6342/NTU202504209

doi:10.6342/NTU202504209

doi:10.6342/NTU202504209

一、緒論 Introduction

1. Essential Tremor (ET)

Essential tremor is the most common cause of a pathological tremor (Sharma & Pandey, 2020), and is known to affect over 60 million worldwide (Welton et al. (2021). Diagnosis of the disease is clinical. Essential tremor was defined as (1) Isolated tremor syndrome of **bilateral upper limb action tremor** at least **3 years'** duration (2) With or without tremor in **other locations** (e.g., head, voice, or lower limbs) (3) **Absence of other neurological signs**, such as dystonia, ataxia, or parkinsonism (Bhatia et al., 2018). Risk factors include aging, exposure to environmental factors (pesticides, heavy metals, dietary factors, smoking), and genetic predisposition (Klaming & Annese, 2014; Welton et al., 2021). Proposed pathophysiologies of ET includes environmental exposures to β-carboline, cerebellar GABA deficiency, climbing fiber synaptic pathology with related cerebellar oscillatory activity, extra-cerebellar oscillatory activity (Pan & Kuo, 2022). Pharmacological therapy included propranolol, primidone, and topiramate. Propranolol and primidone, as the first-line option for treatment of the disease, provide 50% reduction of tremor in those that are responsive (population that are responsive approximates 50% of those treated). Topiramate, which is more commonly used under settings of migraine and seizure management, is efficacious for treatment of essential tremor only if used in >200mg per day. Adverse effects including weight loss, paresthesia, cognitive side effects are common (Hedera et al., 2013). For medication-refractory cases, surgical intervention including deep brain stimulation (DBS), magnetic resonance guided-focused-ultrasound

doi:10.6342/NTU202504209

surgery (MRgFUS) can be considered as alternative ways of tremor reduction (Hedera et al., 2013; Sharma & Pandey, 2020).

2. Pathophysiology of ET

2.1 The cerebello-thalamo-cortical loop

Essential tremor is widely regarded a network disease. Based on electrophysiological and neuroimaging data, a model wherein tremor arises from a widely distributed network involving multiple brain regions identified as nodes, including cerebellum, thalamus, motor cortex, interconnected by pre-lemniscal and corticopontine tracts, and the Guillain-Mollaret triangle is the current model accepted (Welton et al., 2021)(**Figure 1**). The cerebello-thalamo-cortical loop, delineated by these nodes, exhibits abnormality when examined by postmortem, electrophysiological, as well as functional and structural neuroimaging. All nodes of the circuit were found to have altered functional connections, and it is proposed that multiple oscillation generators contribute to the network dysfunction rather than being fueled by one specific oscillator dysfunction. The components of the circuit entrain each other in the generation of ET (Nicoletti et al., 2020; Raethjen & Deuschl, 2012; Younger et al., 2023). The model was supported by studies facilitating techniques including electroencephalogram (EEG) and magnetoencephalogram (MEG), functional magnetic resonance imaging (fMRI), positron emission tomography (PET), transcranial magnetic stimulation (TMS), and transcranial alternative current stimulation (tACS) (Pan & Kuo, 2022; Wills et al., 1994). The network is similar to the therapeutic network derived from lesions improving ET (lesion network mapping), with key regions aligning in the thalamus

doi:10.6342/NTU202504209

and cerebellum (Younger et al., 2023). The instability of the network is in contrast to the relatively stable relay in case of voluntary motor control (Raethjen & Deuschl, 2012).

2.2 The Cerebellum as the Hub of ET Tremor Network

Clinical clues indicate the cerebellum's role in ET pathogenesis. Cerebellar deficits, including intention tremor and tandem gait ataxia, are observed in half of the ET population. Intention tremor of varying severity was identified in almost 60% of ET individuals in a study by Deuschl et al (Deuschl et al., 2000). Abnormalities in tandem gait with an increased number of mis-steps and a broad-based, ataxic and dysmetric gait which was indistinguishable from the findings in cerebellar diseases (Stolze et al., 2001). Alcohol consumption has been observed to lead to improvement of tremor and reduce the number of missteps in patients with ET (Klebe et al., 2005; Mostile & Jankovic, 2010), which may be explained by the influence of alcohol being exerted on alcohol-sensitive gamma-aminobutyric acid receptors within the cerebellum. This should be considered along with the postmortem pathological findings regarding the ET cerebellum. Modest Purkinje cell (which is GABAergic) damages and cell loss was observed in the cerebellar cortex. The deep cerebellar nuclei, which receive GABAergic inputs via Purkinje cells, were found to have reduced number of $GABA_A$ and $GABA_B$ receptors, further diminishing cerebellar GABA transmission. It was thus hypothesized that the oscillatory activity is represented in the cerebellum, and alcohol intake suppressed tremor by enhancing GABA transmission under a state of GABA insufficiency (Pan & Kuo, 2022; Raethjen & Deuschl, 2012). The morphologic alterations of the cerebellar cortex are not limited to Purkinje cells, and include climbing fiber synaptic pathology (which appears to be the most specific change to

doi:10.6342/NTU202504209

ET) as well as abnormal axonal processes of the basket cell surrounding the initial segment of Purkinje cells. Alteration of GABAergic transmissions from the interneurons can greatly alter the firing patterns of the Purkinje cells, thereby affecting the cerebellar oscillations (Pan & Kuo, 2022).

The cerebellum was demonstrated to be functionally connected to other parts of the tremor network in over 90% of studies and significantly different in connectivity compared to the control dataset of other movement disorders (Younger et al., 2023). Connectivity between the cerebellum and the sensorimotor cortices was demonstrated to be significantly reduced in patients with ET. More specifically, the cerebellar hub and the sensorimotor cortices were found to be anticorrelated, whereas they were found to be positively correlated in healthy subjects (Younger et al., 2023). Significant coupling between the contralateral sensorimotor cortex and tremor-related muscle activity in patients with essential tremor was revealed with corticomuscular coherence analyses based on EEG–EMG recordings (Hellwig et al., 2001). In ET patients, functional connectivity between the primary motor cortex (M1) and the contralateral motor cerebellum (lobule IV–V, VI) was found to be decreased, and this connectivity showed a negative correlation with tremor severity (Nicoletti et al., 2020).

These findings depicted the cerebellum hub being “uncoupled” from the rest of the motor network, supposedly contributing to the impairment of refined motor control in ET subjects. Recent studies have demonstrated the cerebellum as the hub of the ET tremor network, in comparison to PD tremor and dystonic tremor, where the basal ganglia is to play a role in pathogenesis (Buijink et al., 2022; Younger et al., 2023).

doi:10.6342/NTU202504209

2.3 Ventral Intermediate (Vim) Nucleus

The ventral intermediate nucleus (VIM) of the thalamus functions as a key site receiving input from the cerebellum. It has been observed that tremor-related neural activity appears in this region across several tremor syndromes, including essential tremor (ET), dystonic tremor, and tremor associated with Parkinson's disease, suggesting overlapping underlying mechanisms (Buijink et al., 2022). The successful suppression of tremor symptoms in ET through targeted lesions within the VIM provides compelling evidence of the thalamus's involvement in producing the aberrant rhythmic activity in this condition (Jankovic et al., 1995; Raethjen & Deuschl, 2012).

While no significant association was found between tremor severity and functional connectivity from the cerebellum to the sensorimotor cortex, positive correlations emerged when examining the connectivity between cerebellar lobule VI and the VIM, as well as between the VIM and sensorimotor regions. These findings lend support to the view that essential tremor arises from dysregulated communication within the cerebello–thalamo–cortical pathway, with the thalamus acting as a central node linking aberrant cerebellar signals to cortical motor regions (Younger et al., 2023).

2.4 Thalamo-cortical Oscillations

Bi-directional thalamo-cortical oscillations have been demonstrated in individuals with essential tremor (ET) through EEG–EMG coherence analysis (Muthuraman et al., 2012). Evidence from single-neuron recordings (Hua et al., 1998) and local field potentials

doi:10.6342/NTU202504209

(Pedrosa et al., 2012) within the thalamus further supports its capacity to function as an intrinsic oscillator. Additionally, the development of postural and kinetic tremor in a patient following ipsilateral cerebellar hemispherectomy suggests that the thalamus may generate oscillatory activity independently of cerebellar input (Chahine & Ghosh, 2009).

Clues of the motor cortex participating in generation of tremor in ET can be seen in successful alteration of the tremor by means of non-invasive modulations. Past studies had either successfully reset tremor with supra-threshold single-pulse transcranial magnetic stimulation of the cortex (Pascual-Leone et al., 1994) or reduced tremor amplitude with inhibitory subthreshold continuous theta-burst stimulation outlasting the stimuli with TMS (Hellriegel et al., 2012). PET studies disclosed overactivity in the cerebellum, contralateral red nucleus, thalamus, and sensorimotor cortex, hinting that the dysfunctional ET network had the cortical region entrained (Wills et al., 1994).

Multiple high-resolution EEG and MEG studies have provided compelling evidence of cortical activity that is coherent with essential tremor (ET) (Hellwig et al., 2001; Pollok et al., 2004; Raethjen et al., 2007). Significant coupling of the contralateral sensorimotor cortex and tremor-related muscle activity supports cortical motor area involvement in the production of ET tremor (Hellwig et al., 2001). Further analyses of temporal delays and directionality between cortical signals (EEG/MEG) and peripheral tremor activity (EMG) suggest that this coherence cannot be solely attributed to sensory feedback. Instead, it reflects genuine rhythmic output from the cortex to the muscles, supporting a direct cortical contribution to tremor generation (Govindan et al., 2006; Schelter et al., 2009). These findings reinforce the notion that the cortex plays an active, though possibly intermittent, role in the genesis of ET (Raethjen & Deuschl, 2012; Raethjen et al., 2007).

doi:10.6342/NTU202504209

Although accumulating evidence suggests the involvement of oscillatory neural activity in essential tremor (ET), no animal models have yet been developed to directly confirm whether such activity is sufficient to generate tremor. Moreover, the absence of post-mortem studies investigating pathological changes in the thalamus or motor cortex leaves the structural basis of ET pathogenesis unresolved (Pan & Kuo, 2022).

3. Functional Organization of Cerebellar Peduncles and Their Major Afferent and Efferent Pathways

The cerebellar peduncles form the principal white matter pathways linking the cerebellum with other brain regions. (Summarized in **Table 1.1 & 1.2**)

The superior cerebellar peduncle (SCP) primarily conveys efferent outputs from the cerebellar deep nuclei. Fibers originating from the dentate, interposed, and fastigial nuclei project via the SCP to the ventrolateral nucleus of the thalamus (VL), red nucleus (parvocellular and magnocellular divisions), and the tectum. Additionally, the ventral and rostral spinocerebellar tracts, which carry proprioceptive information from leg and arm interneurons respectively, also ascend through the SCP as afferent components.

The middle cerebellar peduncle (MCP) consists exclusively of afferent fibers. These are the pontocerebellar fibers, which originate from the cerebral cortex and relay through the pontine nuclei before entering the cerebellum. This corticopontocerebellar pathway plays a critical role in relaying cortical signals necessary for the coordination of skilled voluntary movements.

doi:10.6342/NTU202504209

The inferior cerebellar peduncle (ICP) carries both afferent and efferent fibers. Its afferent tracts include the dorsal spinocerebellar tract (conveying leg proprioceptive signals via the nucleus dorsalis of Clarke), the cuneocerebellar tract (conveying arm proprioception via the external cuneate nucleus), reticulocerebellar and vestibulocerebellar fibers, and climbing fibers from the inferior olivary nucleus, which originate from multiple sources including the red nucleus, cortex, brainstem, and spinal cord. The cerebellovestibular efferent tract also exits the cerebellum through the ICP, projecting back to the vestibular nuclei. (Blumenfeld, 2010; Lingford-Hughes & Kalk, 2012)

4. MR-guided Focused Ultrasound (MRgFUS) Vim thalamotomy in the treatment of ET

Magnetic Resonance-guided Focused Ultrasound (MRgFUS) is a noninvasive thermal ablation technique that utilizes high-frequency ultrasound beams converged onto deep brain targets to induce focal heating. The absorption of acoustic energy results in a rapid temperature rise at the focal point. When the tissue temperature exceeds approximately 55°C, even for a brief period—as short as one second—thermal damage becomes irreversible, primarily through protein denaturation and subsequent coagulative necrosis. The extent of lesioning is determined not only by peak temperature but also by the thermal dose, which reflects both the duration of heating and the volume of tissue exposed.
The procedure is performed under real-time MR thermometry, enabling precise monitoring of the focal temperature to ensure safety and spatial accuracy. In clinical practice, Vim thalamotomy for tremor treatment is executed in a progressive three-stage manner: low-

doi:10.6342/NTU202504209

power sonication is first used to confirm accurate targeting, followed by intermediate energy delivery to assess transient clinical effects. Once optimal targeting is verified, higher-intensity sonication is applied—typically not exceeding 60°C—to achieve durable tissue ablation.

MRgFUS offers a noninvasive alternative to conventional surgical approaches, avoiding craniotomy and implanted hardware, and is particularly suitable for patients with medically refractory tremor (Giordano et al., 2020; Schlesinger et al., 2017). Long-term evaluations indicate that MRgFUS provides durable symptomatic relief in essential tremor, with hand tremor and disability scores reduced by approximately 56–63% at 3- and 4-year follow-ups, and notable improvements in quality of life metrics (Chang et al., 2018; Halpern et al., 2019; Park et al., 2019; Sinai et al., 2020). In two individuals monitored over five years, CRST and QUEST scores remained markedly lower than baseline (Sinai et al., 2020). Nonetheless, a modest rebound in tremor severity and functional impairment was observed at year 3 relative to the 6-month mark, and about 11% of patients experienced symptom recurrence, potentially attributable to disease progression (Halpern et al., 2019; Louis et al., 2011; Sinai et al., 2020). Procedure-related effects such as head pain and dizziness, affecting over one-third of cases, generally resolved within 3 months (Iacopino et al., 2018). Neurologically, ataxia was most frequently reported (50%), followed by sensory alterations (20%), likely linked to inadvertent lesion spread beyond the VIM, whose borders are poorly visualized on conventional MRI, with involvement of adjacent tracts such as the ML and CST (Boutet et al., 2018). Encouragingly, the frequency of these adverse events declined over time, and no new complications were documented with extended follow-up (Chang et al., 2018; Halpern et al., 2019; Park et al., 2019). However,

doi:10.6342/NTU202504209

attrition rates were considerable—reaching 31% at 3 years—posing limitations on the interpretation of late safety outcomes (Chang et al., 2018; Halpern et al., 2019; Park et al., 2019). Importantly, no instances of hemorrhage, seizures, or access-related injuries have been reported, supporting the procedure's favorable risk profile compared to DBS or RFA. A major limitation in assessing the long-term complications of the patients undergoing MRgFUS is the high dropout rate (Agrawal et al., 2021; Kim et al., 2017; Wong et al., 2020).

5. Hypothesis and Goals of this Study

In this study, we investigated different regions of interest (ROIs) using both diffusion tensor imaging (DTI) and voxel-based morphometry (VBM) to comprehensively assess white matter microstructure and regional gray/white matter volume. The ROIs were selected based on their potential involvement in the pathophysiology and treatment outcomes of essential tremor (ET).

We hypothesize that (1) patients with ET exhibit microstructural abnormalities—reflected by alterations in DTI scalar indices—or volumetric changes within the cerebellar peduncles compared to healthy controls (HC), as assessed by cross-sectional analysis; and (2) following therapeutic intervention and subsequent clinical improvement, these microstructural or volumetric characteristics may undergo further modulation, such that post-treatment values differ from pre-treatment baselines, as examined through longitudinal analysis.

In addition, we aimed to explore whether baseline clinical and imaging features are

doi:10.6342/NTU202504209

associated with tremor severity, and whether they may serve as potential predictors of treatment response to MRgFUS thalamotomy.

5.1 Regions of Interest for Cross-sectional and Longitudinal analysis

In the diffusion tensor imaging (DTI) analysis, we first examined the "long tracts"—including the corticospinal tract, frontopontine tract, medial lemniscus, and the M1–Vim projection—given their established roles in motor execution and their potential involvement in both tremor genesis and treatment-related adverse effects. The frontopontine fibers serve as a communication pathway to the opposite cerebellum, allowing for the coordination of planned motor functions (Rea, 2015). Notably, lesions in the frontopontine tract have been associated with tremor resolution (Dupuis et al., 2010), while structural changes in the medial lemniscus and corticospinal tract have been implicated in procedure-related complications.

Second, particular attention was directed toward the cerebellar peduncles—the superior (SCP), middle (MCP), and inferior (ICP)—which serve as the principal afferent and efferent pathways linking the cerebellum to the broader motor network. Given the cerebellum’s central role in the pathophysiology of essential tremor (ET), and accumulating evidence of both GABAergic dysfunction and microstructural abnormalities in cerebellar regions, we hypothesized that these peduncles exhibit disease-related alterations at baseline as well as longitudinal changes following MRgFUS thalamotomy.

Third, the corpus callosum was included to assess potential interhemispheric involvement. Our prior observations have indicated that tremor may worsen in the untreated hand after

doi:10.6342/NTU202504209

unilateral Vim thalamotomy, raising the possibility of altered cross-hemispheric communication mediated by callosal fibers.

To complement the microstructural analysis provided by DTI, voxel-based morphometry (VBM) was employed to assess volumetric changes in both gray and white matter regions associated with tremor generation and control. Cortical ROIs included the pre-supplementary motor area (preSMA), supplementary motor area (SMA), and primary motor cortex (M1), which are critically involved in the planning, initiation, and execution of voluntary movement.

Within the thalamus, we analyzed the ventral intermediate nucleus (Vim) and the ventral lateral posterior nucleus (VLp). The Vim, the primary lesion target of MRgFUS thalamotomy, plays a central role in relaying cerebellar output to motor cortical regions. The VLp, which encompasses the Vim, receives excitatory input from the dentate nucleus and projects broadly to motor and associative cortical areas.

Given converging evidence from pathological and imaging studies suggesting GABAergic dysfunction and functional uncoupling between the cerebellum and motor circuits in ET, we also examined the SCP, MCP, and ICP, as well as the dorsal dentate nucleus, which is the major output nucleus of the cerebellum. The red nucleus was included due to its role as a relay node within the tremor network.

Lastly, the corpus callosum was again assessed in the VBM analysis to further investigate whether altered transcallosal connectivity manifests as macroscopic volumetric changes, potentially reflecting pathological status in ET or following unilateral intervention.

doi:10.6342/NTU202504209

The selection rationale for each ROI and relevant findings from prior studies are presented in the following two sections: Tables 2.1.1 and 2.1.2 summarize the reasons for ROI inclusion, while Tables 2.2.1, 2.2.2, 2.3.1, 2.3.2 compile supporting evidence from previous literature.

5.2 Clinical and Neuroimaging Correlates of Baseline Tremor Severity and Treatment Outcome

Essential tremor (ET) presents with varying degrees of baseline severity, yet most patients undergoing MRgFUS Vim thalamotomy experience meaningful clinical improvement. To better characterize the sources of individual variability, we examined whether baseline clinical factors—such as age at tremor onset, disease duration, and family history—as well as neuroimaging features (DTI/VBM of tremor-related ROIs), are associated with initial tremor severity.

Furthermore, although treatment outcomes were generally favorable, we explored whether certain factors—such as age at treatment, pre-treatment severity, skull density ratio (SDR), and MRgFUS parameters (e.g., energy, temperature, number of sonications)—correlate with the magnitude of clinical improvement. We further investigated whether the volume of tremor-related brain regions prior to treatment correlated with the degree of clinical improvement.

doi:10.6342/NTU202504209

二、研究方法與材料 Methods and Materials

1. Study Population

1.1 Patient Recruitment

This study enrolled patients with essential tremor (ET) who underwent magnetic resonance-guided focused ultrasound (MRgFUS) Vim thalamotomy at China Medical University Hospital (CMUH), Taichung, Taiwan, between June 2019 and October 2024. A total of 20 patients (15 males and 5 females), aged 20 to 74 years, were included. Patients included both newly diagnosed and previously diagnosed cases of ET who were evaluated by board-certified neurologists and deemed suitable candidates for MRgFUS Vim thalamotomy. Among them, two patients were diagnosed with PD-ET overlap syndrome.

All patients underwent unilateral Vim thalamotomy. Except for one left-handed patient who received right-sided thalamotomy, all others were right-handed and received left-sided thalamotomy. One patient underwent a second MRgFUS procedure on the contralateral side two years after the first. One patient received subsequent radiofrequency ablation due to the failure to reach the therapeutic temperature during MRgFUS. Five patients had received prior pharmacological treatment for ET, while the remaining patients were drug-naïve.

Prior to the treatment, all patients underwent brain CT for skull density ratio (SDR) assessment (SDR = 0.5 ± 0.13), and comprehensive clinical evaluations including medical history, medication use, family history, and tremor history. Baseline clinical severity of

doi:10.6342/NTU202504209

tremor was assessed using the Fahn–Tolosa–Marin Tremor Rating Scale (FTM-TRS), and MRI scanning was performed. Most patients underwent follow-up MRI and TRS assessments at multiple timepoints postoperatively (**Table 3.1, 3.2, 4**).

1.2 Postoperative Data Stratification

Postoperative follow-up data were stratified using a generalized estimating equation (GEE) model to determine tremor improvement trajectories based on TRS Part A total scores. Based on the identified temporal pattern of tremor recurrence (**Figure 2**), follow-up MRI data were classified into early postoperative (ET-early, 1 day to 14 months post-surgery) and late postoperative (ET-late, 15 to 61 months post-surgery) phases (**Table 4**). When multiple MRI scans were available within the same time window, the latest MRI and the closest TRS assessment were selected.

A total of 21 preoperative datasets (including two datasets from one patient who underwent surgery twice), 13 ET-early datasets (one without corresponding DTI data), and 8 ET-late datasets were included in the analyses. Four patients were lost to follow-up after baseline evaluation; their preoperative data were only used for ET vs. healthy control (HC) comparisons, and not for longitudinal analyses (**Table 5**).

1.3 Healthy Control Recruitment

doi:10.6342/NTU202504209

A total of 23 age-matched healthy controls (13 males and 10 females) were recruited (**Table 7**). Two-sample t-tests confirmed no significant age differences between ET patients and controls. Controls were recruited from healthy volunteers and neurology outpatients and were screened for electrolyte imbalances, thyroid dysfunction, and abnormal glucose levels. Exclusion criteria included tremor, structural brain abnormalities (e.g., stroke, neurosurgery), neurodegenerative diseases, epilepsy, psychiatric conditions, migraine, chronic pain, diabetes, carotid or transcranial sonography findings indicating >70% stenosis or hemodynamic abnormalities, or abnormal laboratory results. All participants provided written informed consent after receiving a full explanation of the study purpose and procedures.

All controls underwent FTM-TRS assessment and MRI scanning. One subject was excluded from DTI analysis due to orthodontic braces causing imaging artifacts.

2. Tremor Evaluation

2.1 Fahn–Tolosa–Marin Tremor Rating Scale (FTM-TRS)

Tremor severity in both patients and healthy controls was assessed using the FTM-TRS, which consists of three subscales:

- **Part A** evaluates tremor presence and severity at various body locations. (**Figure 4.1**)
- **Part B** rates performance in specific motor tasks (e.g., handwriting, spiral drawing, line drawing, pouring water). (**Figure 4.2**)

doi:10.6342/NTU202504209

- **Part C** measures functional disability caused by tremor. (**Figure 4.3**)

All evaluations were performed by a board-certified neurologist. With participant consent, clinical assessments were video-recorded for documentation and potential future review.

2.2 Selected Tremor Subscores for Treated and Untreated Hands (sel_Rt, sel_Lt)

To improve sensitivity and specificity in assessing hand tremor changes, we constructed composite subscores for each hand using selected FTM items:

- **sel_Rt (Treated Hand)**:
    - Part A, Item 5 (resting, postural, and action/intention tremor of the right upper extremity)
    - Part B, Items 12–14 (right hand: spiral drawings and straight-line drawings)
- **sel_Lt (Untreated Hand)**:
    - Part A, Item 6 (resting, postural, and action/intention tremor of the left upper extremity)
    - Part B, Items 12–14 (left hand: spiral drawings and straight-line drawings)

For patients who underwent **left Vim thalamotomy**, sel_Rt and sel_Lt were transposed such that the treated side consistently corresponded to sel_Rt across all patients.

Excluded Items:

doi:10.6342/NTU202504209

- **Part B, Item 11 (handwriting with dominant hand)** was excluded due to low sensitivity to tremor (as handwriting performance may remain relatively preserved).
- **Part B, Item 15 (pouring water from a cup)** was excluded due to low specificity and inconsistencies in administration (e.g., varying cup height, lid presence).
- Other Part A items not involving hand tremor were also excluded.

3 MRI Processing

3.1 MRI Specifications

All patients and healthy controls underwent MRI scanning. Patients received scans at baseline (pre-MRgFUS) and at postoperative time points, while control participants underwent a single MRI scan.

MRI was performed using a SIGNA Architect 3T scanner (GE Healthcare, Milwaukee, WI, USA) equipped with a 48-channel head coil. Whole-brain 3D T1-weighted SPGR images were acquired in the axial plane with a voxel size of $1 \times 1 \times 1$ mm³. Diffusion-weighted imaging (DWI) was conducted using spin-echo echo-planar imaging (EPI) with the following parameters: matrix size = 96×96; 56 axial slices; voxel size = $2.5 \times 2.5 \times 2.5$ mm³; 1 NEX; hyperband acceleration factor = 2. The diffusion protocol included 50 isotropically distributed directions with a b-value of 1500 s/mm² and 5 non-diffusion-weighted (b0) volumes.

doi:10.6342/NTU202504209

3.2 MRI Data Processing

3.2.1 Mask Editing

Most region-of-interest (ROI) masks used in this study were directly extracted from standardized MNI-space atlases, including **AAL3**, **HCP842**, **JHU white-matter atlas**, **Brainnetome**, **HCP-MMP**, **HCPex**, **JulichBrain**, and **THOMAS**. These masks were used for subsequent imaging analyses to investigate region-specific features. Due to differences in coverage and definition across atlases, two distinct masks of the **inferior cerebellar peduncle (ICP)**—one from the **HCP-482 atlas** and one from the **JHU atlas**—were both included in the analysis.

The **superior cerebellar peduncle (SCP)** and **middle cerebellar peduncle (MCP)** were manually edited using **FSLeyes**, as only bilateral masks were available in the source atlases (**Figure 3.1, Figure 3.2.1 & 3.2.2**). The MCP was divided along the midline into left and right hemispheric masks, while the SCP was diagonally split. The resulting unilateral masks remained in MNI space and were subsequently transformed into native space using **inverse deformation fields** generated from tissue segmentation and spatial normalization of individual T1-weighted structural images via **CAT12.9 (r2577)**. This transformation ensured consistent and anatomically aligned ROI definitions across imaging modalities (e.g., VBM and DTI).

Additionally, because the corpus callosum in the selected atlas was segmented into subregions (genu, body, and splenium), these were manually merged in FSLeyes into a single unified mask (**corpus_callosum_combined**) for use in later analyses.

doi:10.6342/NTU202504209

3.2.2 Diffusion Tensor Imaging (DTI)

The DTI ROIs included the **corticospinal tract, frontopontine tract, medial lemniscus, M1–Vim projection, superior cerebellar peduncle (SCP), middle cerebellar peduncle (MCP),** and **inferior cerebellar peduncle (ICP)**. Tractography and extraction of scalar indices were performed using **DSI Studio (2024, Chen edition; PC platform)**. For all ROIs except the M1–Vim projection, scalar values were extracted based on atlas-derived or manually edited ROI masks.

For the M1–Vim projections, tractography was performed using atlas-defined **M1** (primary motor cortex) and **Vim** (ventral intermediate nucleus of the thalamus) as the seed and target regions. The tracking parameters were set as follows: tracking index = FA; angular threshold = 30°; step length = 0 mm; minimum/maximum length = 30–200 mm; termination after 3000 tracts; topology-informed pruning = 16; autotrack tolerance = 24 mm.

3.2.3 Voxel-Based Morphometry (VBM)

VBM analysis was performed using **CAT12.9 (r2577)**. ROIs included the **pre-supplementary motor area (preSMA), supplementary motor area (SMA), primary motor cortex (M1), ventral intermediate (Vim), ventral anterior (VA), ventral lateral posterior (VLp) thalamic nuclei, SCP, MCP, ICP, dorsal dentate nucleus**, and **red nucleus**. ROI-based analyses were conducted using both standard atlas-defined masks in MNI space and subject-specific masks derived from manual editing and tractography.

doi:10.6342/NTU202504209

4. Statistical Analysis

4.1 Longitudinal Change in Tremor Severity After MRgFUS Vim Thalamotomy

To evaluate longitudinal changes in tremor severity following MRgFUS Vim thalamotomy across all patients—and to define postoperative MRI follow-up as either early (ET-early) or late (ET-late) based on the timing of clinical tremor recurrence—we employed Generalized Estimating Equations (GEE) to model the change in total tremor score (FTM-TRS Part A) relative to baseline. This approach allowed us to integrate discrete timepoint assessments into a population-averaged trend model.

To account for the potentially non-linear evolution of tremor severity over time, postoperative follow-up periods were categorized into the following intervals: Category 0 (Baseline), 1 (1 day post-treatment), 2 (1 month), 3 (2–3 months), 4 (4–6 months), 5 (7–14 months), and 6 (≥15 months). These categories were included as predictors alongside a continuous time variable and its squared term to capture linear and non-linear trends. Interaction terms were used to examine whether the rate of change varied across follow-up intervals.

In addition to the total tremor score, we constructed separate GEE models for the total score of selected items for the treated hand (sel_Rt) and its change from baseline. To control for overall tremor burden, the untreated hand tremor score (sel_Lt) was included as a covariate after mean-centering (sel_Lt_c). This allowed us to model the treated-hand trajectory

doi:10.6342/NTU202504209

assuming average untreated-hand severity, thereby facilitating interpretation of treatment-specific effects.

Based on statistical analyses (described in detail in Sections 4.1.1–4.1.3 and Section 4.2) and the prediction curve derived from the GEE model of the change in FTM-TRS Part A total score, we defined the early post-treatment (ET-early) period as 0–14 months after treatment and the late post-treatment (ET-late) period as 15–61 months after treatment.

In the early post-treatment phase (n = 13), total TRS scores were significantly reduced from baseline (Mean = 48.31, SD = 18.37) to early post-treatment (Mean = 25.15, SD = 12.19), $p < .001$, with a mean reduction of 23.15 points (95% CI: 17.04 to 29.27), indicating a statistically significant improvement in overall tremor severity. Tremor scores for the treated hand improved significantly from baseline (Mean = 14.08, SD = 3.86) to early post-treatment (Mean = 6.23, SD = 2.92), $p < .001$, with a mean reduction of 7.85 points (95% CI: 5.83 to 9.86), reflecting a robust treatment effect. In contrast, tremor scores for the non-treated hand showed no significant difference between baseline (Mean = 11.54, SD = 5.46) and early post-treatment (Mean = 10.62, SD = 5.36), $p = .213$, with a mean reduction of 0.92 points (95% CI: –0.61 to 2.45).

In the late post-treatment phase (n = 7), total TRS scores remained significantly improved compared with baseline, decreasing from a baseline mean of 52.14 (SD = 15.16) to 34.29 (SD = 9.25), $p = .006$, with a mean reduction of 17.86 points (95% CI: 7.43 to 28.29), suggesting a sustained treatment effect over time. Tremor scores for the treated hand also showed a significant reduction from baseline (Mean = 14.57, SD = 2.57) to late post-treatment (Mean = 8.29, SD = 2.36), $p = .003$, with a mean reduction of 6.29 points (95%

doi:10.6342/NTU202504209

CI: 3.01 to 9.56), indicating a lasting benefit on the treated side. However, tremor scores for the non-treated hand did not differ significantly between baseline (Mean = 12.71, SD = 4.89) and late post-treatment (Mean = 14.57, SD = 4.86), p = .258, with a mean increase of 1.86 points (95% CI: –5.50 to 1.78), suggesting a possible slight worsening of tremor severity on the non-treated side, although the change did not reach statistical significance compared with baseline.

4.1.1 Longitudinal Analysis of Change in FTM-TRS Part A Total Score

GEE models were used to analyze changes in total FTM-TRS Part A scores over time. Key predictors included:

- *Timeintervalm_ad*: a continuous variable representing months since treatment;
- *TRS_category_num*: a categorical variable representing the follow-up time interval;
- *TRS_category_num#Timeintervalm_ad*: an interaction term assessing time trends within each category;
- *time_sq*: the squared term of time to model non-linear changes in symptom trajectory.

Initial models included all terms, and model reduction was performed based on statistical significance (Wald test, p > 0.05). An exchangeable working correlation structure was specified for GEE estimation. Predicted values and 95% confidence intervals were generated using predictnl, based on empirically observed combinations of *Timeintervalm_ad* and *TRS_category_num*. Implausible or unobserved combinations were excluded. Curves

doi:10.6342/NTU202504209

were annotated with predicted values at representative timepoints. The origin (0,0) was optionally added to graphs to reflect change from baseline.

4.1.2 Longitudinal Analysis of FTM-TRS Selected Item Scores for the Treated Hand

A similar GEE framework was used to analyze total scores of selected FTM items for the treated hand (sel_Rt). In addition to time variables (*Timeintervalm_ad*, *TRS_category_num*, *time_sq*, and interaction terms), this model included the centered untreated-hand score (*sel_Lt_c*) and its interaction terms with time variables to account for baseline tremor severity.

Predicted values and confidence intervals were computed using predictnl, with *sel_Lt_c* fixed at zero (i.e., average untreated-hand score). Predicted population-level trends were plotted and annotated at empirically observed timepoints.

4.1.3 Longitudinal Analysis of Change in FTM-TRS Selected Item Scores for the Treated Hand

GEE models were also used to analyze the change in sel_Rt score from baseline (Δsel_Rt = Post-treatment – Baseline), following the same modeling procedure as in section 4.1.2.

doi:10.6342/NTU202504209

4.2 Sensitivity Analysis

In the original dataset, each of the two patients undergoing bilateral thalamotomy contributed two sets of observations (corresponding to their first and second procedures), which were treated as independent cases. This approach violated the assumption of independence between subjects. Given the relatively small sample size, the inclusion of these duplicated observations—each representing a second-side procedure—may have introduced bias and unduly influenced the model estimates by violating the assumption of subject-level independence. To assess the robustness and reliability of the findings, a sensitivity analysis was conducted. Compared to the original model, the sensitivity model excluded data from the second-side procedures of these two patients (ET001L and ET010R).

Beta coefficients (β) and standard errors (SE) from both the main and sensitivity models were compared. The difference in coefficients ($\Delta\beta = \beta_1 - \beta_2$), along with the corresponding 95% confidence intervals (CIs), was calculated under the assumption of independence. Variables with CIs that did not include zero were considered significantly affected by case duplication.

The differences in coefficients (Beta_Diff) between the sensitivity models (**Tables 9.1–9.3**) and the original generalized estimating equation (GEE) models (**Tables 8.1–8.3**) across all examined variables were subsequently compared and visualized (**Figure 6**).

doi:10.6342/NTU202504209

Note: To maintain balanced group sizes across time intervals, ET010R's follow-up MRI—conducted at 7 months post-treatment—was categorized under *TRS_category_num = 4* (i.e., the 4–6 month interval) in both the original and sensitivity GEE models.

5. Cross-Sectional Comparison (ET vs. HC)

Following the temporal classification determined by the GEE models described above, postoperative MRI data from essential tremor (ET) patients were stratified into early (ET-early) and late (ET-late) phases. Cross-sectional comparisons were then conducted between ET patients at three time points (baseline/preoperative, early postoperative, and late postoperative) and healthy controls (HC) to assess group-level differences in voxel-based morphometry (VBM) and diffusion tensor imaging (DTI) metrics across predefined regions of interest (ROIs).

Multiple linear regression models were employed to evaluate group effects, controlling for age, sex, and total Fahn–Tolosa–Marin tremor rating scale (FTM-TRS) score, which served as a proxy for overall disease severity. Separate analyses were conducted for ROIs corresponding to the treated hemisphere, non-treated hemisphere, and corpus callosum. To account for multiple comparisons, false discovery rate (FDR) correction was applied using the Benjamini–Hochberg procedure across all ROI sets, except for those within the corpus callosum. All statistical analyses were performed using Stata/BE 17.0 (StataCorp, College Station, TX, USA).

doi:10.6342/NTU202504209

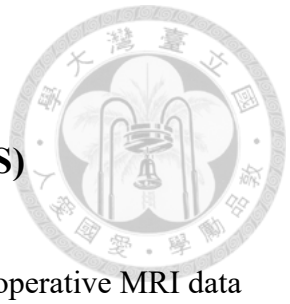

6. Longitudinal Comparison (ET After vs. Before MRgFUS)

Based on the temporal boundaries identified through GEE analysis, postoperative MRI data from ET patients were categorized into ET-early and ET-late groups. Two longitudinal comparisons were performed: (1) ET-early versus ET-baseline (preoperative), and (2) ET-late versus ET-baseline. These analyses aimed to examine intra-individual changes in brain structure following MRgFUS treatment, focusing on VBM and DTI metrics across selected ROIs.

Paired linear regression models were used to assess longitudinal differences, adjusting for age, sex, total FTM-TRS score to account for disease severity. As with cross-sectional comparisons, analyses were stratified by ROI location (treated hemisphere, non-treated hemisphere, and corpus callosum). FDR correction using the Benjamini–Hochberg method was applied to all ROI comparisons except those involving the corpus callosum. All analyses were conducted using Stata/BE 17.0 (StataCorp, College Station, TX, USA).

7. Clinical Correlation

7.1 Association Between Tremor Severity and Clinical Characteristics

doi:10.6342/NTU202504209

To explore the relationship between preoperative clinical and neuroimaging variables and tremor severity prior to MRgFUS thalamotomy, a series of statistical analyses were conducted using Stata/BE 17.0 (StataCorp, College Station, TX, USA).

7.1.1 Demographic and Clinical Predictors

Multiple linear regression models were employed to examine the association between tremor severity—measured using the total FTM-TRS score and selected item scores for the treated (sel_Rt) and non-treated (sel_Lt) hands—and clinical predictors including age at tremor onset, age at operation, disease duration, family history of tremor, and skull density ratio (SDR). All models were adjusted for sex.

7.1.2 Association Between Baseline Regional Volume and Tremor Severity

To assess the structural correlates of tremor severity, region-wise multiple linear regression analyses were performed using preoperative voxel-based morphometry (VBM) measures. Each model included the volume of a single region of interest (ROI) as the independent variable, with tremor severity scores (TRS, sel_Rt, sel_Lt) as outcomes. Age and sex were included as covariates. Correction for multiple comparisons was performed using the Benjamini–Hochberg False Discovery Rate (FDR) method.

doi:10.6342/NTU202504209

7.1.3 Association Between Baseline DTI Metrics and Tremor Severity

Cross-sectional linear regression analyses were conducted to evaluate the relationship between diffusion tensor imaging (DTI) scalar indices—fractional anisotropy (FA) and mean diffusivity (MD)—and tremor severity scores. Each ROI's DTI value was entered into a separate model as the predictor, adjusting for age and sex. FDR correction was applied across all models to account for multiple testing.

7.2 Predictors of Outcome Following MRgFUS Thalamotomy

To identify predictors of clinical response following MRgFUS Vim thalamotomy, we evaluated the association between preoperative clinical variables, intraoperative treatment parameters, and imaging measures with percentage improvement in tremor scores. All statistical analyses were conducted using Stata/BE 17.0 (StataCorp, College Station, TX, USA).

7.2.1 Clinical Predictors of Treatment Response

Linear mixed-effects models with restricted maximum likelihood (REML) estimation were used to examine the association between clinical characteristics—including age at operation, age at tremor onset, disease duration, family history, SDR, and follow-up timepoint (early vs. late)—and percentage improvement in tremor outcomes

doi:10.6342/NTU202504209

(TRS_%improved, sel_Rt%improved, sel_Lt%improved). Random intercepts at the subject level were included to account for repeated measures.

7.2.2 Intraoperative MRgFUS Parameters

To evaluate the relationship between treatment parameters and clinical improvement, linear mixed-effects models were fitted using the following sonication metrics as predictors: maximum energy delivered, peak power (maximum wattage), maximum focal temperature achieved, and the total number of treatment sonications. The outcome variables were percentage improvements in TRS, sel_Rt, and sel_Lt scores. Subject-specific random intercepts were included to account for within-subject correlations.

7.2.3 Baseline ROI Volume and Treatment Response

Separate ROI-wise linear regression analyses were performed to assess whether baseline gray matter volume in specific regions was predictive of percentage improvement in tremor severity following MRgFUS. Each ROI was analyzed in an individual model with adjustment for age and sex. To control for multiple testing, the Benjamini–Hochberg FDR method was applied across all ROI comparisons.

doi:10.6342/NTU202504209

三、研究結果 Results

1. Longitudinal change in tremor severity after MRgFUS Vim thalamotomy

This study demonstrated significant and sustained reductions in tremor severity following unilateral MRgFUS, as reflected in both the FTM-TRS Part A total score change and change in selected tremor items TRS score in the treated hand. Improvements were most prominent within the first month post-treatment and remained stable through extended follow-up. The baseline tremor score of the dominant hand (mean = 13.5) was significantly higher than that of the non-dominant hand (mean = 11.0), with a mean difference of 2.52 points (p = 0.006).

1.1 Longitudinal Analysis of FTM-TRS Part A Total Score Change

The GEE model showed significant tremor improvement at Day 1 (β = −4.685, $p < 0.001$), Month 1 (β = −3.724, $p < 0.001$), and beyond Month 15 (β = −7.48, $p = 0.001$), compared to baseline. The continuous time effect (Timeintervalm_ad) approached significance ($p = 0.058$), suggesting a mild trend of decreasing benefit over time. Interaction and quadratic time terms were not significant, indicating no distinct rate differences or non-linear trends across time intervals. The overall model fit was moderate (Chi-square = 55.706) (**Table 8.1**).

doi:10.6342/NTU202504209

The prediction curve derived from this model showed a rapid initial decrease in tremor severity, followed by a plateau. Improvement was defined as the post-treatment total score minus the baseline total score. This trend was supported by the significance of the quadratic term and the dense clustering of follow-ups in the early phase. Based on the predicted curve (**Figure 2**), clinical tremor recurrence was estimated to occur approximately 17 months after treatment. Accordingly, postoperative MRI data were stratified into early postoperative (ET-early, 0–14 months) and late postoperative (ET-late, ≥15 months) phases based on the timing of each patient's follow-up MRI (**Table 4, 5**). The histogram illustrating the percentage of tremor improvement in the early and late post-treatment stages is presented in **Figure 5.1 & 5.2**, and the descriptive statistics (mean, maximum, minimum, and standard deviation) for each group are provided in **Table 6.**

1.2 Longitudinal Analysis of FTM-TRS Selected Item Scores of the Treated Hand

The GEE model revealed a significant overall reduction in selected tremor item scores over time (Timeintervalm_ad: $\beta = 0.739$, $p = 0.006$), though this effect must be interpreted in the context of time categorization and interaction terms. Significant improvements were found at Day 1 ($\beta = -8.709$), Month 1 ($\beta = -8.292$), Months 7–14 ($\beta = -9.128$), and ≥15 months ($\beta = -17.454$), all $p < 0.05$, indicating robust short- and long-term efficacy.

A significant time interaction was noted at Months 4–6 ($\beta = -3.898$, $p = 0.026$). Baseline tremor in the untreated hand (sel_Lt_c) was positively associated with treated-hand tremor scores ($\beta = 0.477$, $p < 0.001$), suggesting that greater overall tremor burden was linked to

doi:10.6342/NTU202504209

worse treated-hand outcomes. However, its interaction with time was not significant. The significant negative quadratic term (β = −0.01, $p = 0.005$) supports a nonlinear trajectory, with initial rapid improvement followed by slower change. The model showed good fit (Chi-square = 475.132, $p < 0.001$) (**Table 8.2**).

1.3 Longitudinal Analysis of Change in FTM-TRS Selected Item Scores of the Treated Hand

The GEE model showed significant improvement in tremor scores at Day 1 (β = −8.424), Month 1 (β = −7.626), and ≥15 months (β = −15.209), all $p < 0.01$, as well as at Months 7–14 (β = −10.063, $p = 0.047$). The continuous time variable approached significance ($p = 0.06$), suggesting a slight decrease in improvement over time. The quadratic term also trended toward significance (β = −0.007, $p = 0.074$), indicating a possible nonlinear trajectory. Interaction terms and sel_Lt_c were not significant. Overall, early and late effects were more stable, while mid-term effects were less consistent. Model fit was moderate (Chi-square = 273.520) (**Table 8.3**).

This pattern mirrored that seen in Part A total score, with early gains tapering over time. Improvement was defined as the post-treatment minus baseline sel_Rt score. The model adjusted for untreated-hand tremor (sel_Lt_c), fixed at the group mean in all predictions to isolate the group-level trend.

doi:10.6342/NTU202504209

1.4 Sensitivity Analysis

A comparison between the original models (Table 6.1–6.3) and the sensitivity models (Table 7.2–7.4) revealed largely consistent results across most variables (Table 7.1), supporting the robustness of the main analysis. However, a notable discrepancy was observed for the variable **TRS_category_num_4**, which corresponds to the 4–6 month post-treatment interval. The differences in regression coefficients (Beta_Diff) between the original and sensitivity GEE models across all examined variables are illustrated in **Figure 6.**

It is important to note that in our study, the classification of post-MRgFUS MRI scans into early (ET-early) and late (ET-late) stages was based on longitudinal changes in TRS-part A scores, rather than fixed time intervals. Therefore, this discrepancy does not affect subsequent analyses in this study.

Specifically:

- In the **sel_Rt model** (total tremor score of the treated hand), the coefficient for TRS_category_num_4 shifted from a positive value (+12.5) in the original model—suggesting symptom worsening—to a negative value (–11.4) in the sensitivity model, indicating symptom improvement.
- In the **sel_Rtimproved model** (percentage tremor improvement, calculated as (baseline–post−MRgFUS)/baseline×100(baseline – post-MRgFUS) / baseline × 100%(baseline–post−MRgFUS)/baseline×100), the coefficient also reversed

doi:10.6342/NTU202504209

direction, from –85.1 (implying substantial worsening) to +80.3 (suggesting marked improvement).

This directional reversal indicates that inclusion of second-side procedure data in the original model may have introduced bias, potentially inflating tremor severity or underestimating clinical improvement in the 4–6 month post-treatment period. After excluding these duplicated data points, the sensitivity model yielded a more consistent and clinically plausible estimate, reflecting sustained therapeutic benefit during this interval.

These findings suggest that the sensitivity model offers a more conservative and reliable estimation of treatment effects during the 4–6 month postoperative period.

2. Cross-Sectional Comparison (ET vs. HC)

2.1 DTI

In the comparison between ET patients and healthy controls, no significant DTI differences were identified. In the early post-treatment phase, ET patients demonstrated increased FA in the frontopontine tract associated with the non-treated hand. No significant changes were observed in the ROIs associated with the treated hand. The corpus callosum as a whole exhibited increased FA; regionally, increased FA was noted in the genu, body, and splenium, with the splenium also showing decreased MD. In the late post-treatment phase, no significant differences were detected in the ROIs corresponding to the non-treated hand,

doi:10.6342/NTU202504209

treated hand, or corpus callosum compared with healthy controls (**Table 11.1-11.3, 13.1-13.3, 15.1-15.3**).

2.2 VBM

In the comparison between ET patients and healthy controls, voxel-based morphometry revealed that the left inferior cerebellar peduncle (L_ICP, HCP482 atlas) associated with the nondominant hand had significantly greater volume in ET patients (Coef = 0.105, p = 0.0244). For the dominant hand, greater volume was observed in the right middle cerebellar peduncle (R_MCP; Coef = 0.096, p = 0.0400) and the right inferior cerebellar peduncle (R_ICP, HCP482 atlas; Coef = 0.082, p = 0.0256) in ET group. No significant differences were found in the corpus callosum (**Table 11.1-11.3**).

In the early post-treatment phase, ET patients exhibited greater volume in the left dorsal dentate nucleus associated with the non-treated hand (Coef = 0.041, p = 0.0159), whereas the right dorsal dentate nucleus associated with the treated hand showed reduced volume (Coef = –0.035, p = 0.0252) compared with healthy controls. No significant differences were observed in the corpus callosum (**Table 13.1-13.3**).

In the late post-treatment phase, no significant volumetric differences were detected in the ROIs corresponding to the non-treated hand, treated hand, or corpus callosum compared with healthy controls (**Table 15.1-15.3**).

doi:10.6342/NTU202504209

3. Longitudinal Comparison (ET After vs. Before MRgFUS)

3.1 DTI

In the longitudinal comparison between ET patients and their baseline scans, no significant DTI changes were observed in the early post-treatment phase for ROIs associated with the non-treated hand, treated hand, or corpus callosum. In the late post-treatment phase, a significant reduction in FA was detected in the right inferior cerebellar peduncle (R_ICP, JHU atlas) associated with the treated hand (Coef = –0.037, p = 0.0315), while no significant changes were observed in the ROIs corresponding to the non-treated hand or corpus callosum (**Table 16.1-16.3, 18.1- 18.3**).

3.2 VBM

In the longitudinal VBM analysis, the early post-treatment phase showed a significant volume reduction in the right red nucleus associated with the non-treated hand compared with baseline (Coef = –0.004, p = 0.0271). No significant changes were observed in the ROIs corresponding to the treated hand or corpus callosum. In the late post-treatment phase, compared with baseline, the treated hand showed volume reductions in the right middle cerebellar peduncle (R_MCP; Coef = –0.043, p = 0.256) and the right inferior cerebellar peduncle (R_ICP, HCP482 atlas; Coef = –0.049, p = 0.0240). No significant differences were detected in the ROIs associated with the non-treated hand or corpus callosum (**Table 17.1-17.3, 19.1- 19.3**).

doi:10.6342/NTU202504209

4. Summary of the cross-sectional and longitudinal analysis

Summary tables are available **(Table 20.1 – 20.4).**

5. Clinical correlation

5.1 Association Between Tremor Severity and Clinical Characteristics

5.1.1 Age at Onset, Family History, Disease Duration, age at operation, SDR (skull density ratio)

Older onset age correlated positively with greater overall tremor severity (TRS) (Coef = 0.545, $p < 0.05$) and with greater tremor severity of the dominant hand (sel_Rt) (Coef = 0.152, $p < 0.01$). Disease duration was positively associated only with tremor severity of the dominant hand (sel_Rt) (Coef = 0.209, $p < 0.05$) and showed no significant correlation with tremor severity of the non-dominant hand (sel_Lt) or overall tremor severity (TRS). Both older onset age (Coef = 0.152, $p < 0.01$) and longer disease duration (Coef = 0.209, $p < 0.05$) were positively correlated with greater dominant hand tremor severity. Family history showed no significant correlation with tremor severity（**Table 21.1**).

5.1.2 Baseline volume of ROIs

doi:10.6342/NTU202504209

Bilateral VLp and the left Vim were positively correlated with tremor severity of the non-dominant hand (sel_Lt) (Coef = –1069.078, p = 0.044). Specifically, the left VLp (Coef = 24.148, p = 0.046), right VLp (Coef = 26.486, p = 0.038), and left Vim (Coef = 22.712, p = 0.026) each showed significant positive correlations with sel_Lt. Further analysis in the healthy control group revealed that the right VLp had significantly greater gray matter volume than the left VLp (mean difference = –0.023, 95% CI = [–0.035, –0.011], p < 0.001). In contrast, no significant volumetric difference was observed between the left and right Vim in healthy controls (left Vim mean = 0.533, right Vim mean = 0.536, mean difference = –0.003, p = 0.5838) **(Table 21.2- 21.4)**.

5.1.3 Baseline DTI scalar values of ROIs

At baseline, no ROI showed a significant association between DTI scalar values and tremor severity **(Table 21.5- 21.7).**

5.2 Predictors of Outcome Following MRgFUS thalamotomy

5.2.1 Association Between Improvement of TRS score (In Percentage) and Clinical Characteristics

Advanced age at the time of treatment was associated with greater improvement in overall tremor severity (TRS) after treatment (Coef = 0.720, p < 0.05), with no significant benefit observed for tremor improvement in either hand. Baseline disease burden (TRS) correlated inversely with improvement in overall tremor severity (Coef = –0.612, p < 0.05) and

doi:10.6342/NTU202504209

showed no significant correlation with improvement in tremor of either hand. Baseline tremor severity of the treated hand was not significantly correlated with its percentage of improvement following treatment. Family history of tremor correlated positively with improvement in overall tremor severity (TRS) (Coef = 24.461, $p < 0.05$), whereas no significant difference in the percentage of tremor reduction was observed in either hand. Patients with a family history of tremor demonstrated greater improvement in overall tremor severity and tremor severity of the non-treated hand compared with those without a family history (n = 2), while improvement in tremor of the treated hand did not differ between the two groups. A longer time interval between treatment and TRS evaluation correlated inversely with the percentage of improvement in overall tremor severity (Coef = –0.450, $p < 0.01$) and in tremor of the non-treated hand (Coef = –0.870, $p < 0.001$). No significant correlation was found between time interval and tremor deterioration in the treated hand**. (Table 22.1)**

5.2.2 Association Between Improvement of TRS score (In Percentage) and MRgFUS Parameters

None of the MRgFUS treatment parameters analyzed showed a significant association with tremor improvement after adjusting for timepoint as an independent covariate. **(Table 22.2)**

5.2.3 Association Between Improvement of TRS score (In Percentage) and ROI Volume

doi:10.6342/NTU202504209

No predictor was found for tremor severity (TRS total score, sel_Rt, sel_Lt) **(Table 22.3-22.5**).

5.3 Summary of Predictors Associated with Tremor Improvement in Treated and Non-Treated Hands

See **Table 23.1 & 23.2.**

doi:10.6342/NTU202504209

四、討論 Discussion

1. Longitudinal change in tremor severity after MRgFUS Vim thalamotomy

MRgFUS provides rapid, durable, and unilateral tremor control in essential tremor. Modeled predictions and graphical trajectories confirm that most therapeutic benefit occurs within the first month and is maintained thereafter.

While tremor severity in the untreated hand (sel_Lt) was significantly correlated with absolute tremor scores in the treated hand (sel_Rt), it was not predictive of change in tremor score of the right hand after MRgFUS. That is to say, while baseline contralateral tremor severity may reflect systemic burden, it does not predict treatment responsiveness on the treated side, further supporting the localized, unilateral clinical effect of MRgFUS thalamotomy.

2. DTI and VBM: Cross-sectional and Longitudinal Comparisons

The diagnosis of essential tremor (ET) is primarily based on clinical criteria. In contrast to neurodegenerative diseases such as Alzheimer's disease and Parkinson's disease, where the distribution of pathological changes follows well-characterized patterns and diagnosis can be confirmed post-mortem (Braak & Braak, 1991; Braak et al., 2003), there are currently no definitive radiological or pathological markers for ET. Identifying structural characteristics

doi:10.6342/NTU202504209

of ET on MRI could enhance our understanding of the disease and move its diagnosis beyond purely clinical grounds.

In this study, although no significant differences were observed in DTI indices between essential tremor (ET) patients and healthy controls (HC) in cross-sectional comparisons, longitudinal within-subject analyses (early vs. baseline) revealed significant microstructural changes across multiple regions. This discrepancy may be attributable to differences in statistical design. Longitudinal comparisons, being within-subject, control for inter-individual variability and thus offer greater statistical power to detect subtle changes. In contrast, cross-sectional comparisons are more susceptible to between-group heterogeneity and reduced sensitivity. Moreover, baseline DTI indices in ET patients were likely comparable to those of HC, making postoperative changes more detectable when compared against each patient's own pre-treatment status.

In the ET-early vs. HC comparison, all corpus callosum subregions (genu, body, splenium) demonstrated increased FA, with the splenium additionally showing decreased MD. These findings may reflect a microstructural compensatory adjustment in interhemispheric connectivity during the early post-tremor onset phase, potentially aimed at improving motor coordination. Following MRgFUS, the integration of motor and sensory information between the two hemispheres may have been enhanced.

DTI changes were also observed in the right frontopontine tract (controlling the left hand), which may indicate adaptive motor control reorganization for the non-dominant hand after surgery. In the early postoperative period, patients might experience mild worsening of tremor in the non-dominant (left) hand or an increased demand for compensatory

doi:10.6342/NTU202504209

modulation. The brain may recruit non-dominant hemisphere motor pathways to maintain balanced bilateral motor output.

By the late postoperative stage (>14 months), no significant differences were found between ET-late and HC, suggesting that the early microstructural remodeling is a temporary and plastic process rather than a permanent injury or irreversible degeneration. These DTI changes may represent a temporary regulatory mechanism that gradually resolves as clinical symptoms stabilize and the nervous system re-establishes equilibrium, indicating that the system has completed adaptation and integration without the need for sustained recruitment of compensatory tracts.

In the longitudinal comparison of ET-late vs. baseline, a reduction in FA was observed in pathways reliant on input from the inferior cerebellar peduncle (ICP) for tremor correction. This may indicate a decreased demand for ICP-mediated sensory input over the long term. Following treatment, the functional emphasis of cerebellar network activity may shift away from an overreliance on external sensory input conveyed through the ICP. Such a redistribution of network weighting could lead to structural weakening in previously hyperactive pathways, as reflected by the observed DTI changes.

Bilateral enlargement of the inferior cerebellar peduncles (ICPs) may represent an “amplification” or compensatory hypertrophy of sensory feedback pathways. The ICP serves as a critical hub for integrating sensory inputs, receiving spinovestibular signals, and contributing to postural control and error correction during movement by integrating proprioceptive and vestibular information.

doi:10.6342/NTU202504209

Such volumetric increases may suggest that patients with ET rely excessively on sensory input for movement correction during tremor. This finding supports the view that ET represents a dysfunction of the broader sensorimotor network rather than an isolated motor pathway abnormality. Chronic enlargement of the ICPs could reflect a sustained demand for tremor-related motor adjustments, leading to long-term compensatory thickening of these sensory feedback tracts.

Additionally, the increased volume of the middle cerebellar peduncle (MCP) on the dominant-hand side may indicate greater involvement of cortical motor input pathways (via the MCP) in tremor pathophysiology. This asymmetry could be related to the more frequent use and greater symptom severity of the dominant hand, even when tremor is present in both hands.

3. Clinical Correlation

3.1 Association Between Tremor Severity and Clinical Characteristics

In our study, we observed that patients with later onset of essential tremor (ET) exhibited greater overall tremor severity (TRS) and more severe dominant-hand tremor (sel_Rt) compared with those with earlier onset, after controlling for disease duration. This finding suggests that symptom progression is faster in late-onset ET, which is consistent with previous reports. Notably, in our cohort, nearly all treated patients had an age at onset > 60 years, which aligns with the “late-onset” group definition in prior studies (Gironell et al.,

doi:10.6342/NTU202504209

2015; Louis et al., 2000). Although the correlation coefficient between age at onset and dominant-hand tremor severity was higher than that for the non-dominant hand, the difference did not reach statistical significance due to large inter-individual variability (non-dominant hand: r = 0.111, SE = 0.084; dominant hand: r = 0.152, SE = 0.048). To our knowledge, prior studies examining the association between age at onset and tremor severity have not separately analyzed dominant and non-dominant hands, and thus comparative data in this regard are lacking.

We also found that longer disease duration was associated with more severe dominant-hand tremor (sel_Rt), but not with overall tremor severity (TRS) or non-dominant hand tremor (sel_Lt). This suggests that ET generally follows a slow disease course, and when controlling for age at onset and family history, progression over time is less pronounced. The observed dominant-hand–specific effect may reflect more frequent use of the dominant hand, which, through neuroplastic changes, could strengthen tremor-related circuits and amplify disease duration effects (coef = 0.209, $p < 0.05$). This same mechanism may also explain why baseline tremor scores were slightly higher in the dominant hand compared with the non-dominant hand (mean = 13.5 vs. 11.0; mean difference = 2.52, p = 0.006).

Finally, we did not identify a significant association between family history of ET and tremor severity. However, interpretation is limited by sampling bias, as most patients in our series reported a positive family history (only two patients without).

doi:10.6342/NTU202504209

In this study, we found that the volumes of both VLp and the left Vim were positively correlated with non-dominant hand tremor severity (sel_Lt) (L_VLp: Coef = 24.148, p = 0.046; R_VLp: Coef = 26.486, p = 0.038; L_Vim: Coef = 22.712, p = 0.026). Further analysis of the healthy control (HC) group revealed that the right VLp had significantly greater gray matter volume than the left VLp (mean difference = –0.023, 95% CI = [–0.035, –0.011], p < 0.001), whereas no significant volumetric difference was observed between the left and right Vim (left Vim mean = 0.533; right Vim mean = 0.536; mean difference = –0.003, p = 0.584).

Previous studies have shown that patients with dystonic tremor have larger VLp volumes than HCs, with corresponding tremor-related activity detected in this region. The VLp is a major recipient of output signals from the cerebellar dentate nucleus, and the Vim nucleus constitutes part of the VLp. It remains unclear whether the enlarged VLp observed in dystonic tremor is directly related to its abnormal pathophysiology, as the authors have not provided a definitive explanation (Nieuwhof et al., 2022) .

In our comparison of ET baseline with HC, no significant VLp volumetric differences were identified, making it uncertain whether similar enlargement to that reported in dystonic tremor would emerge with a larger sample size and greater statistical power. Additionally, in the ET baseline group, the left VLp exhibited significantly smaller VBM values than the right VLp (mean difference = –0.023, p < 0.001), whereas no significant volumetric asymmetry was found for the Vim (mean difference = –0.0012, 95% CI = –0.0151 to 0.0127, p = 0.861). The reason for the observed left–right asymmetry in VLp volume remains unclear. The lack of detectable volume differences in the Vim may be partly

doi:10.6342/NTU202504209

attributable to its relatively small anatomical size, which increases susceptibility to partial volume effects and limits the sensitivity of voxel-based morphometry to detect subtle structural changes. In contrast, the larger volume and broader anatomical extent of the VLp may facilitate the detection of volumetric differences, potentially explaining why significant associations were observed in the VLp but not in the Vim.

Regarding disease course and time-related factors, no significant association was found between the time interval from treatment to TRS evaluation (months) and tremor deterioration in the treated hand, suggesting that the therapeutic effect remained relatively stable and, based on the present evidence, was not influenced by the length of the follow-up interval. Patients with greater overall disease burden at baseline (higher baseline TRS total scores) demonstrated less overall tremor improvement after treatment; however, baseline TRS was not significantly associated with tremor improvement in either hand individually. This may reflect that such patients experienced smaller improvements in functional disability (TRS part C) or less improvement in tremor affecting non-hand body parts. Regression analysis showed no significant correlation between improvement in TRS part C and baseline TRS (coefficient = –0.230, p = 0.575) (**Table 24.1**).

Age at the time of treatment showed a certain association with symptom improvement. When calculated using the TRS total score, older patients demonstrated greater improvement, which may be related to a heightened perception of benefit or greater satisfaction with tremor reduction in this age group, potentially introducing subjective bias in scoring. To verify this hypothesis, TRS part C (patient self-reported assessment) was

doi:10.6342/NTU202504209

excluded, and regression was repeated using the sum of part A and part B scores only. The results showed no significant association between the improvement in part A + part B total scores and age at the time of treatment (**Table 24.2**). This suggests that the greater TRS total score improvement observed in older patients was primarily attributable to subjective improvements in daily functioning (part C), whereas objective motor performance did not differ significantly from that of younger patients. Consistently, age at the time of treatment was significantly positively correlated with improvement in TRS part C (coefficient = 1.790, $p < 0.01$) (**Table 24.1**), further supporting this interpretation.

Conversely, baseline TRS was not significantly correlated with improvement in part A + part B total scores (**Table 24.2),** but was significantly negatively correlated with improvement in TRS total scores (coefficient = –0.612, $p = 0.037$) (**Table 22.1**). This suggests that patients with higher baseline TRS may have more limited improvement in part C or less improvement in tremor affecting non-hand regions; however, this association could not be definitively confirmed.

Neither SDR nor treatment parameters were significantly associated with clinical outcomes, indicating that, in the present study, the patient group had SDR values within the appropriate range and that the process of achieving lesioning was not a major determinant of treatment efficacy.

With regard to family history, patients with a positive family history (the majority of our cohort) demonstrated greater improvement in overall tremor severity and in tremor severity of the non-treated hand compared with those without a family history (n = 2), while

doi:10.6342/NTU202504209

improvement in the treated hand did not differ between groups. Given the small number of patients without a family history, the interpretability of this finding is limited.

doi:10.6342/NTU202504209

五、本研究的限制 Limitations

Several limitations in the present study should be acknowledged.

First, technical constraints in MRI data processing may have limited the sensitivity to detect microstructural changes, particularly in regions with complex fiber architecture. The cerebellar peduncles—especially the middle cerebellar peduncle (MCP) and superior cerebellar peduncle (SCP)—are densely populated with crossing fibers from multiple tracts, including the frontopontine, corticopontine, and pontocerebellar pathways (in the MCP), and the dentatorubrothalamic tract (in the SCP). Traditional diffusion tensor imaging (DTI), which relies on tensor-based models, often fails to accurately resolve fiber orientations in such regions. As a result, microstructural changes may be averaged out or underestimated in fractional anisotropy (FA) and mean diffusivity (MD) measurements. The use of more advanced diffusion models such as neurite orientation dispersion and density imaging (NODDI), constrained spherical deconvolution (CSD), or fixel-based analysis (FBA) may provide better sensitivity in future investigations.

Second, structural changes at the voxel level may have been too subtle to be detected by voxel-based morphometry (VBM). The neuropathological features of ET—such as Purkinje cell loss or GABAergic dysfunction—are microscopic and may not translate into detectable gray matter volume changes using standard VBM methods. Thus, while our imaging findings provide insights at a macrostructural level, they may underestimate underlying cellular or neurochemical alterations.

doi:10.6342/NTU202504209

Third, limitations in clinical assessment and study design may have introduced bias or reduced statistical power. Tremor severity ratings (TRS scores) were not obtained through blinded assessments, which may have introduced subjective bias. Additionally, the relatively small sample size limited our ability to detect subtle volumetric differences or group-level effects, particularly in the late follow-up group where attrition was high. The time intervals for late follow-up assessments were also variable across participants, introducing potential heterogeneity within the group. Moreover, cross-sectional comparisons between ET and healthy controls may have been affected by within-group variability and limited statistical power, making it difficult to detect subtle between-group differences.

In future work, increasing the sample size, reducing variability in follow-up timing, and applying more advanced diffusion modeling techniques may enhance the ability to detect clinically and biologically meaningful changes in both microstructure and morphology. Integrating other modalities, such as functional MRI or PET, may also provide complementary information on network-level or metabolic alterations associated with ET and its treatment.

doi:10.6342/NTU202504209

參考文獻 References

Agrawal, M., Garg, K., Samala, R., Rajan, R., Naik, V., & Singh, M. (2021). Outcome and Complications of MR Guided Focused Ultrasound for Essential Tremor: A Systematic Review and Meta-Analysis. *Front Neurol*, *12*, 654711. https://doi.org/10.3389/fneur.2021.654711

Bhatia, K. P., Bain, P., Bajaj, N., Elble, R. J., Hallett, M., Louis, E. D., Raethjen, J., Stamelou, M., Testa, C. M., & Deuschl, G. (2018). Consensus Statement on the classification of tremors. from the task force on tremor of the International Parkinson and Movement Disorder Society. *Mov Disord*, *33*(1), 75-87. https://doi.org/10.1002/mds.27121

Blumenfeld, H. (2010). *Neuroanatomy through clinical cases* (Second Edition ed.). Sinauer Associates, Inc.

Boutet, A., Ranjan, M., Zhong, J., Germann, J., Xu, D., Schwartz, M. L., Lipsman, N., Hynynen, K., Devenyi, G. A., Chakravarty, M., Hlasny, E., Llinas, M., Lozano, C. S., Elias, G. J. B., Chan, J., Coblentz, A., Fasano, A., Kucharczyk, W., Hodaie, M., & Lozano, A. M. (2018). Focused ultrasound thalamotomy location determines clinical benefits in patients with essential tremor. *Brain*, *141*(12), 3405-3414. https://doi.org/10.1093/brain/awy278

Buijink, A. W. G., van Rootselaar, A. F., & Helmich, R. C. (2022). Connecting tremors - a circuits perspective. *Curr Opin Neurol*, *35*(4), 518-524. https://doi.org/10.1097/WCO.0000000000001071

doi:10.6342/NTU202504209

Chahine, L. M., & Ghosh, D. (2009). Essential tremor after ipsilateral cerebellar hemispherectomy: support for the thalamus as the central oscillator. *J Child Neurol*, *24*(7), 861-864. https://doi.org/10.1177/0883073808329528

Chang, J. W., Park, C. K., Lipsman, N., Schwartz, M. L., Ghanouni, P., Henderson, J. M., Gwinn, R., Witt, J., Tierney, T. S., Cosgrove, G. R., Shah, B. B., Abe, K., Taira, T., Lozano, A. M., Eisenberg, H. M., Fishman, P. S., & Elias, W. J. (2018). A prospective trial of magnetic resonance-guided focused ultrasound thalamotomy for essential tremor: Results at the 2-year follow-up. *Ann Neurol*, *83*(1), 107-114. https://doi.org/10.1002/ana.25126

Deuschl, G., Wenzelburger, R., Löffler, K., Raethjen, J., & Stolze, H. (2000). Essential tremor and cerebellar dysfunction clinical and kinematic analysis of intention tremor. *Brain*, *123 (Pt 8)*, 1568-1580. https://doi.org/10.1093/brain/123.8.1568

Dupuis, M. J., Evrard, F. L., Jacquerye, P. G., Picard, G. R., & Lermen, O. G. (2010). Disappearance of essential tremor after stroke. *Mov Disord*, *25*(16), 2884-2887. https://doi.org/10.1002/mds.23328

Dyke, J. P., Cameron, E., Hernandez, N., Dydak, U., & Louis, E. D. (2017). Gray matter density loss in essential tremor: a lobule by lobule analysis of the cerebellum. *Cerebellum Ataxias*, *4*, 10. https://doi.org/10.1186/s40673-017-0069-3

Gallea, C., Popa, T., García-Lorenzo, D., Valabregue, R., Legrand, A. P., Marais, L., Degos, B., Hubsch, C., Fernández-Vidal, S., Bardinet, E., Roze, E., Lehéricy, S., Vidailhet, M., & Meunier, S. (2015). Intrinsic signature of essential tremor in the cerebello-frontal network. *Brain*, *138*(Pt 10), 2920-2933. https://doi.org/10.1093/brain/awv171

doi:10.6342/NTU202504209

Giordano, M., Caccavella, V. M., Zaed, I., Foglia Manzillo, L., Montano, N., Olivi, A., & Polli, F. M. (2020). Comparison between deep brain stimulation and magnetic resonance-guided focused ultrasound in the treatment of essential tremor: a systematic review and pooled analysis of functional outcomes. *J Neurol Neurosurg Psychiatry*, *91*(12), 1270-1278. https://doi.org/10.1136/jnnp-2020-323216

Gironell, A., Ribosa-Nogué, R., Gich, I., Marin-Lahoz, J., & Pascual-Sedano, B. (2015). Severity stages in essential tremor: a long-term retrospective study using the glass scale. *Tremor Other Hyperkinet Mov (N Y)*, *5*, 299. https://doi.org/10.7916/d8dv1hqc

Govindan, R. B., Raethjen, J., Arning, K., Kopper, F., & Deuschl, G. (2006). Time delay and partial coherence analyses to identify cortical connectivities. *Biol Cybern*, *94*(4), 262-275. https://doi.org/10.1007/s00422-005-0045-5

Halpern, C. H., Santini, V., Lipsman, N., Lozano, A. M., Schwartz, M. L., Shah, B. B., Elias, W. J., Cosgrove, G. R., Hayes, M. T., McDannold, N., Aldrich, C., Eisenberg, H. M., Gandhi, D., Taira, T., Gwinn, R., Ro, S., Witt, J., Jung, N. Y., Chang, J. W.,…Ghanouni, P. (2019). Three-year follow-up of prospective trial of focused ultrasound thalamotomy for essential tremor. *Neurology*, *93*(24), e2284-e2293. https://doi.org/10.1212/wnl.0000000000008561

Hedera, P., Cibulčík, F., & Davis, T. L. (2013). Pharmacotherapy of essential tremor. *J Cent Nerv Syst Dis*, *5*, 43-55. https://doi.org/10.4137/jcnsd.S6561

Hellriegel, H., Schulz, E. M., Siebner, H. R., Deuschl, G., & Raethjen, J. H. (2012). Continuous theta-burst stimulation of the primary motor cortex in essential tremor. *Clin Neurophysiol*, *123*(5), 1010-1015. https://doi.org/10.1016/j.clinph.2011.08.033

doi:10.6342/NTU202504209

Hellwig, B., Häussler, S., Schelter, B., Lauk, M., Guschlbauer, B., Timmer, J., & Lücking, C. H. (2001). Tremor-correlated cortical activity in essential tremor. *Lancet*, *357*(9255), 519-523. https://doi.org/10.1016/s0140-6736(00)04044-7

Hua, S. E., Lenz, F. A., Zirh, T. A., Reich, S. G., & Dougherty, P. M. (1998). Thalamic neuronal activity correlated with essential tremor. *J Neurol Neurosurg Psychiatry*, *64*(2), 273-276. https://doi.org/10.1136/jnnp.64.2.273

Iacopino, D. G., Gagliardo, C., Giugno, A., Giammalva, G. R., Napoli, A., Maugeri, R., Graziano, F., Valentino, F., Cosentino, G., D'Amelio, M., Bartolotta, T. V., Catalano, C., Fierro, B., Midiri, M., & Lagalla, R. (2018). Preliminary experience with a transcranial magnetic resonance-guided focused ultrasound surgery system integrated with a 1.5-T MRI unit in a series of patients with essential tremor and Parkinson's disease. *Neurosurg Focus*, *44*(2), E7. https://doi.org/10.3171/2017.11.Focus17614

Jankovic, J., Cardoso, F., Grossman, R. G., & Hamilton, W. J. (1995). Outcome after stereotactic thalamotomy for parkinsonian, essential, and other types of tremor. *Neurosurgery*, *37*(4), 680-686; discussion 686-687. https://doi.org/10.1227/00006123-199510000-00011

Kim, M., Jung, N. Y., Park, C. K., Chang, W. S., Jung, H. H., & Chang, J. W. (2017). Comparative Evaluation of Magnetic Resonance-Guided Focused Ultrasound Surgery for Essential Tremor. *Stereotact Funct Neurosurg*, *95*(4), 279-286. https://doi.org/10.1159/000478866

doi:10.6342/NTU202504209

Klaming, R., & Annese, J. (2014). Functional anatomy of essential tremor: lessons from neuroimaging. *AJNR Am J Neuroradiol*, *35*(8), 1450-1457. https://doi.org/10.3174/ajnr.A3586

Klebe, S., Stolze, H., Grensing, K., Volkmann, J., Wenzelburger, R., & Deuschl, G. (2005). Influence of alcohol on gait in patients with essential tremor. *Neurology*, *65*(1), 96-101. https://doi.org/10.1212/01.wnl.0000167550.97413.1f

Klein, J. C., Lorenz, B., Kang, J. S., Baudrexel, S., Seifried, C., van de Loo, S., Steinmetz, H., Deichmann, R., & Hilker, R. (2011). Diffusion tensor imaging of white matter involvement in essential tremor. *Hum Brain Mapp*, *32*(6), 896-904. https://doi.org/10.1002/hbm.21077

Krauss, J., Upadhyay, N., Purrer, V., Borger, V., Daamen, M., Maurer, A., Schmeel, C., Radbruch, A., Wüllner, U., & Boecker, H. (2025). Beyond the cerebello-thalamo-cortical tract: Remote structural changes after VIM-MRgFUS in essential tremor. *Parkinsonism Relat Disord*, *132*, 107318. https://doi.org/10.1016/j.parkreldis.2025.107318

Lin, C. H., Chen, C. M., Lu, M. K., Tsai, C. H., Chiou, J. C., Liao, J. R., & Duann, J. R. (2013). VBM Reveals Brain Volume Differences between Parkinson's Disease and Essential Tremor Patients. *Front Hum Neurosci*, *7*, 247. https://doi.org/10.3389/fnhum.2013.00247

Lingford-Hughes, A., & Kalk, N. (2012). 2 - Clinical neuroanatomy. In P. Wright, J. Stern, & M. Phelan (Eds.), *Core Psychiatry (Third Edition)* (pp. 13-34). W.B. Saunders. https://doi.org/https://doi.org/10.1016/B978-0-7020-3397-1.00002-1

doi:10.6342/NTU202504209

Louis, E. D., Agnew, A., Gillman, A., Gerbin, M., & Viner, A. S. (2011). Estimating annual rate of decline: prospective, longitudinal data on arm tremor severity in two groups of essential tremor cases. *J Neurol Neurosurg Psychiatry*, *82*(7), 761-765. https://doi.org/10.1136/jnnp.2010.229740

Louis, E. D., Ford, B., & Barnes, L. F. (2000). Clinical subtypes of essential tremor. *Arch Neurol*, *57*(8), 1194-1198. https://doi.org/10.1001/archneur.57.8.1194

Mostile, G., & Jankovic, J. (2010). Alcohol in essential tremor and other movement disorders. *Mov Disord*, *25*(14), 2274-2284. https://doi.org/10.1002/mds.23240

Muthuraman, M., Heute, U., Arning, K., Anwar, A. R., Elble, R., Deuschl, G., & Raethjen, J. (2012). Oscillating central motor networks in pathological tremors and voluntary movements. What makes the difference? *Neuroimage*, *60*(2), 1331-1339. https://doi.org/10.1016/j.neuroimage.2012.01.088

Nicoletti, G., Manners, D., Novellino, F., Condino, F., Malucelli, E., Barbiroli, B., Tonon, C., Arabia, G., Salsone, M., Giofre, L., Testa, C., Lanza, P., Lodi, R., & Quattrone, A. (2010). Diffusion tensor MRI changes in cerebellar structures of patients with familial essential tremor. *Neurology*, *74*(12), 988-994. https://doi.org/10.1212/WNL.0b013e3181d5a460

Nicoletti, V., Cecchi, P., Pesaresi, I., Frosini, D., Cosottini, M., & Ceravolo, R. (2020). Cerebello-thalamo-cortical network is intrinsically altered in essential tremor: evidence from a resting state functional MRI study. *Sci Rep*, *10*(1), 16661. https://doi.org/10.1038/s41598-020-73714-9

Nieuwhof, F., Toni, I., Dirkx, M. F., Gallea, C., Vidailhet, M., Buijink, A. W. G., van Rootselaar, A. F., van de Warrenburg, B. P. C., & Helmich, R. C. (2022).

doi:10.6342/NTU202504209

Cerebello-thalamic activity drives an abnormal motor network into dystonic tremor. *Neuroimage Clin*, *33*, 102919. https://doi.org/10.1016/j.nicl.2021.102919

Pan, M. K., & Kuo, S. H. (2022). Essential tremor: Clinical perspectives and pathophysiology. *J Neurol Sci*, *435*, 120198. https://doi.org/10.1016/j.jns.2022.120198

Park, Y. S., Jung, N. Y., Na, Y. C., & Chang, J. W. (2019). Four-year follow-up results of magnetic resonance-guided focused ultrasound thalamotomy for essential tremor. *Mov Disord*, *34*(5), 727-734. https://doi.org/10.1002/mds.27637

Pascual-Leone, A., Valls-Solé, J., Toro, C., Wassermann, E. M., & Hallett, M. (1994). Resetting of essential tremor and postural tremor in Parkinson's disease with transcranial magnetic stimulation. *Muscle Nerve*, *17*(7), 800-807. https://doi.org/10.1002/mus.880170716

Pedrosa, D. J., Reck, C., Florin, E., Pauls, K. A., Maarouf, M., Wojtecki, L., Dafsari, H. S., Sturm, V., Schnitzler, A., Fink, G. R., & Timmermann, L. (2012). Essential tremor and tremor in Parkinson's disease are associated with distinct 'tremor clusters' in the ventral thalamus. *Exp Neurol*, *237*(2), 435-443. https://doi.org/10.1016/j.expneurol.2012.07.002

Pietracupa, S., Bologna, M., Bharti, K., Pasqua, G., Tommasin, S., Elifani, F., Paparella, G., Petsas, N., Grillea, G., Berardelli, A., & Pantano, P. (2019). White matter rather than gray matter damage characterizes essential tremor. *Eur Radiol*, *29*(12), 6634-6642. https://doi.org/10.1007/s00330-019-06267-9

Pineda-Pardo, J. A., Martínez-Fernández, R., Rodríguez-Rojas, R., Del-Alamo, M., Hernández, F., Foffani, G., Dileone, M., Máñez-Miró, J. U., De Luis-Pastor, E.,

doi:10.6342/NTU202504209

Vela, L., & Obeso, J. A. (2019). Microstructural changes of the dentato-rubro-thalamic tract after transcranial MR guided focused ultrasound ablation of the posteroventral VIM in essential tremor. *Hum Brain Mapp*, *40*(10), 2933-2942. https://doi.org/10.1002/hbm.24569

Pollok, B., Gross, J., Dirks, M., Timmermann, L., & Schnitzler, A. (2004). The cerebral oscillatory network of voluntary tremor. *J Physiol*, *554*(Pt 3), 871-878. https://doi.org/10.1113/jphysiol.2003.051235

Prasad, S., Pandey, U., Saini, J., Ingalhalikar, M., & Pal, P. K. (2019). Atrophy of cerebellar peduncles in essential tremor: a machine learning-based volumetric analysis. *Eur Radiol*, *29*(12), 7037-7046. https://doi.org/10.1007/s00330-019-06269-7

Prasad, S., Rastogi, B., Shah, A., Bhalsing, K. S., Ingalhalikar, M., Saini, J., Yadav, R., & Pal, P. K. (2018). DTI in essential tremor with and without rest tremor: Two sides of the same coin? *Mov Disord*, *33*(11), 1820-1821. https://doi.org/10.1002/mds.27459

Raethjen, J., & Deuschl, G. (2012). The oscillating central network of Essential tremor. *Clin Neurophysiol*, *123*(1), 61-64. https://doi.org/10.1016/j.clinph.2011.09.024

Raethjen, J., Govindan, R. B., Kopper, F., Muthuraman, M., & Deuschl, G. (2007). Cortical involvement in the generation of essential tremor. *J Neurophysiol*, *97*(5), 3219-3228. https://doi.org/10.1152/jn.00477.2006

Rea, P. (2015). *Essential Clinical Anatomy of the Nervous System*. Academic Press. https://doi.org/https://doi.org/10.1016/B978-0-12-802030-2.00010-8

doi:10.6342/NTU202504209

Revuelta, G., McGill, C., Jensen, J. H., & Bonilha, L. (2019). Characterizing Thalamo-Cortical Structural Connectivity in Essential Tremor with Diffusional Kurtosis Imaging Tractography. *Tremor Other Hyperkinet Mov (N Y)*, *9*. https://doi.org/10.7916/tohm.v0.690

Saini, J., Bagepally, B. S., Bhatt, M. D., Chandran, V., Bharath, R. D., Prasad, C., Yadav, R., & Pal, P. K. (2012). Diffusion tensor imaging: tract based spatial statistics study in essential tremor. *Parkinsonism Relat Disord*, *18*(5), 477-482. https://doi.org/10.1016/j.parkreldis.2012.01.006

Schelter, B., Timmer, J., & Eichler, M. (2009). Assessing the strength of directed influences among neural signals using renormalized partial directed coherence. *J Neurosci Methods*, *179*(1), 121-130. https://doi.org/10.1016/j.jneumeth.2009.01.006

Schlesinger, I., Sinai, A., & Zaaroor, M. (2017). MRI-Guided Focused Ultrasound in Parkinson's Disease: A Review. *Parkinsons Dis*, *2017*, 8124624. https://doi.org/10.1155/2017/8124624

Sharma, S., & Pandey, S. (2020). Treatment of essential tremor: current status. *Postgrad Med J*, *96*(1132), 84-93. https://doi.org/10.1136/postgradmedj-2019-136647

Sinai, A., Nassar, M., Eran, A., Constantinescu, M., Zaaroor, M., Sprecher, E., & Schlesinger, I. (2020). Magnetic resonance-guided focused ultrasound thalamotomy for essential tremor: a 5-year single-center experience. *J Neurosurg*, *133*(2), 417-424. https://doi.org/10.3171/2019.3.Jns19466

Stolze, H., Petersen, G., Raethjen, J., Wenzelburger, R., & Deuschl, G. (2001). The gait disorder of advanced essential tremor. *Brain*, *124*(Pt 11), 2278-2286. https://doi.org/10.1093/brain/124.11.2278

doi:10.6342/NTU202504209

Tantik Pak, A., Şengül, Y., Otcu Temur, H., & Alkan, A. (2021). Impaired integrity of commissural and association fibers in essential tremor patients: Evidence from a diffusion tensor imaging study. *Turk J Med Sci*, *51*(1), 328-334. https://doi.org/10.3906/sag-2004-305

Thaler, C., Tian, Q., Wintermark, M., Ghanouni, P., Halpern, C. H., Henderson, J. M., Airan, R. D., Zeineh, M., Goubran, M., Leuze, C., Fiehler, J., Butts Pauly, K., & McNab, J. A. (2023). Changes in the Cerebello-Thalamo-Cortical Network After Magnetic Resonance-Guided Focused Ultrasound Thalamotomy. *Brain Connect*, *13*(1), 28-38. https://doi.org/10.1089/brain.2021.0157

Tikoo, S., Pietracupa, S., Tommasin, S., Bologna, M., Petsas, N., Bharti, K., Berardelli, A., & Pantano, P. (2020). Functional disconnection of the dentate nucleus in essential tremor. *J Neurol*, *267*(5), 1358-1367. https://doi.org/10.1007/s00415-020-09711-9

Welton, T., Cardoso, F., Carr, J. A., Chan, L. L., Deuschl, G., Jankovic, J., & Tan, E. K. (2021). Essential tremor. *Nat Rev Dis Primers*, *7*(1), 83. https://doi.org/10.1038/s41572-021-00314-w

Wills, A. J., Jenkins, I. H., Thompson, P. D., Findley, L. J., & Brooks, D. J. (1994). Red nuclear and cerebellar but no olivary activation associated with essential tremor: a positron emission tomographic study. *Ann Neurol*, *36*(4), 636-642. https://doi.org/10.1002/ana.410360413

Wong, J. K., Hess, C. W., Almeida, L., Middlebrooks, E. H., Christou, E. A., Patrick, E. E., Shukla, A. W., Foote, K. D., & Okun, M. S. (2020). Deep brain stimulation in essential tremor: targets, technology, and a comprehensive review of clinical

doi:10.6342/NTU202504209

outcomes. *Expert Rev Neurother*, *20*(4), 319-331. https://doi.org/10.1080/14737175.2020.1737017

Younger, E., Ellis, E. G., Parsons, N., Pantano, P., Tommasin, S., Caeyenberghs, K., Benito-León, J., Romero, J. P., Joutsa, J., & Corp, D. T. (2023). Mapping Essential Tremor to a Common Brain Network Using Functional Connectivity Analysis. *Neurology*, *101*(15), e1483-e1494. https://doi.org/10.1212/wnl.0000000000207701

doi:10.6342/NTU202504209

附錄

Figures

Figure 1. Schematic representation of the cerebello-thalamo-cortical network involved in essential tremor.

Essential tremor (ET) is now widely considered a network disorder characterized by abnormal oscillatory activity within a distributed cerebello-thalamo-cortical circuit. This schematic illustrates key white matter tracts interconnecting major anatomical nodes implicated in tremor generation. The **blue line** indicates the **cortico-pontine tract**, a key component of the corticopontocerebellar pathway that connects the cerebral cortex to the pontine nuclei and plays a crucial role in coordinating planned movements and motor behavior. The **purple line** represents the **pre-lemniscal radiation**, which conveys ascending sensory and motor signals by traversing the posterior subthalamic area and connecting to motor-related regions including the primary and supplementary motor cortices, orbitofrontal cortex, ventrolateral thalamus, globus pallidus, cerebellum, and dorsal brainstem. The **red line** marks the **Guillain–Mollaret triangle**, a triangular circuit linking the dentate nucleus, red nucleus, and inferior olivary nucleus, important for motor coordination and control; abnormalities in this loop have been associated with various neurological disorders. The **green line** depicts the **spino-cerebellar tract**, which relays unconscious proprioceptive input from the spinal cord to the cerebellum, supporting coordination and postural balance. The **yellow line** represents other interconnecting white matter tracts that facilitate communication among motor-related brain regions. Together,

doi:10.6342/NTU202504209

these pathways form a network believed to underlie tremor generation in ET through pathological entrainment among multiple interconnected nodes.

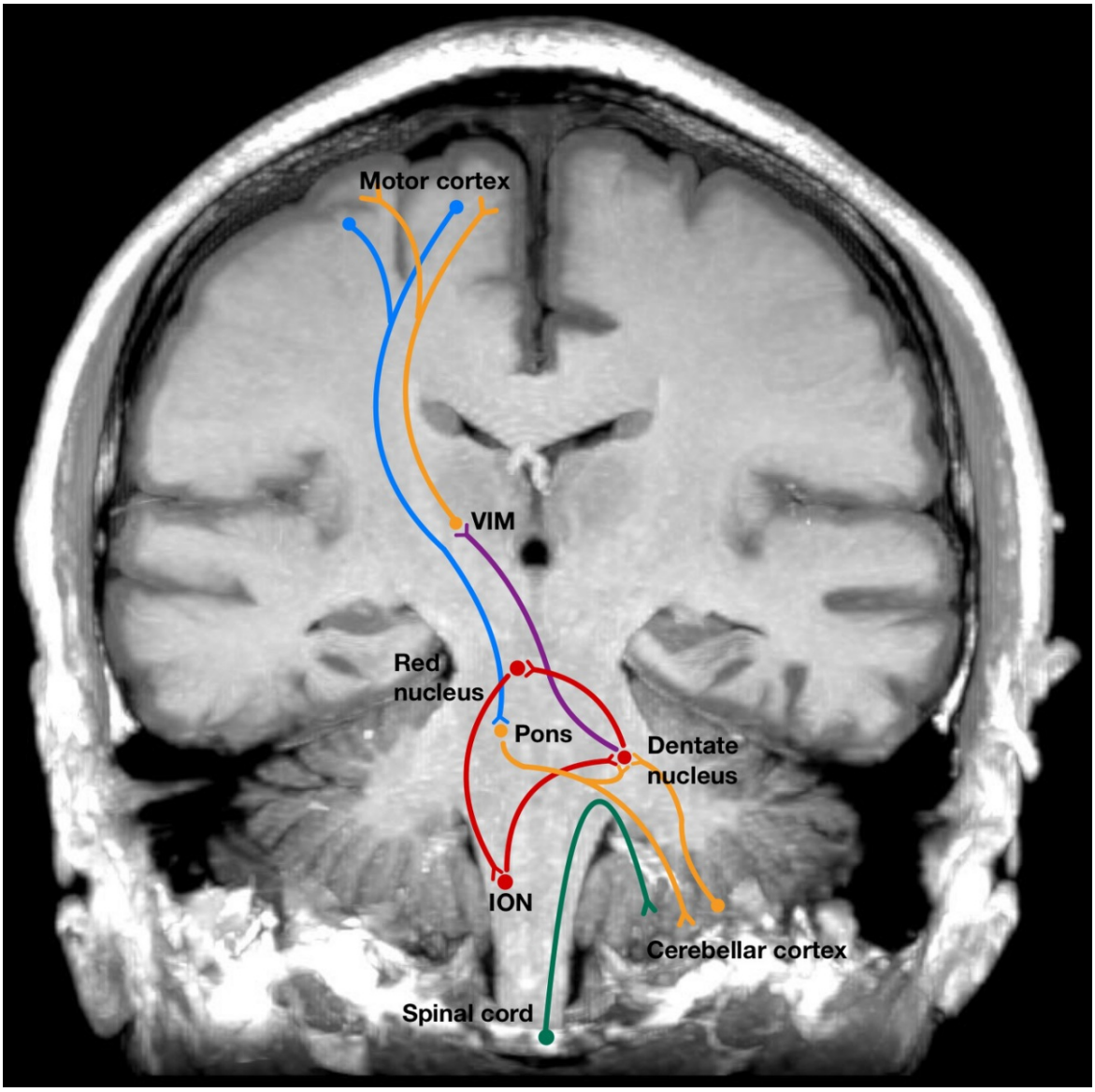

doi:10.6342/NTU202504209

Figure 2. GEE model–based prediction of longitudinal change in FTM-TRS Part A total score (postoperative minus baseline) across timepoints

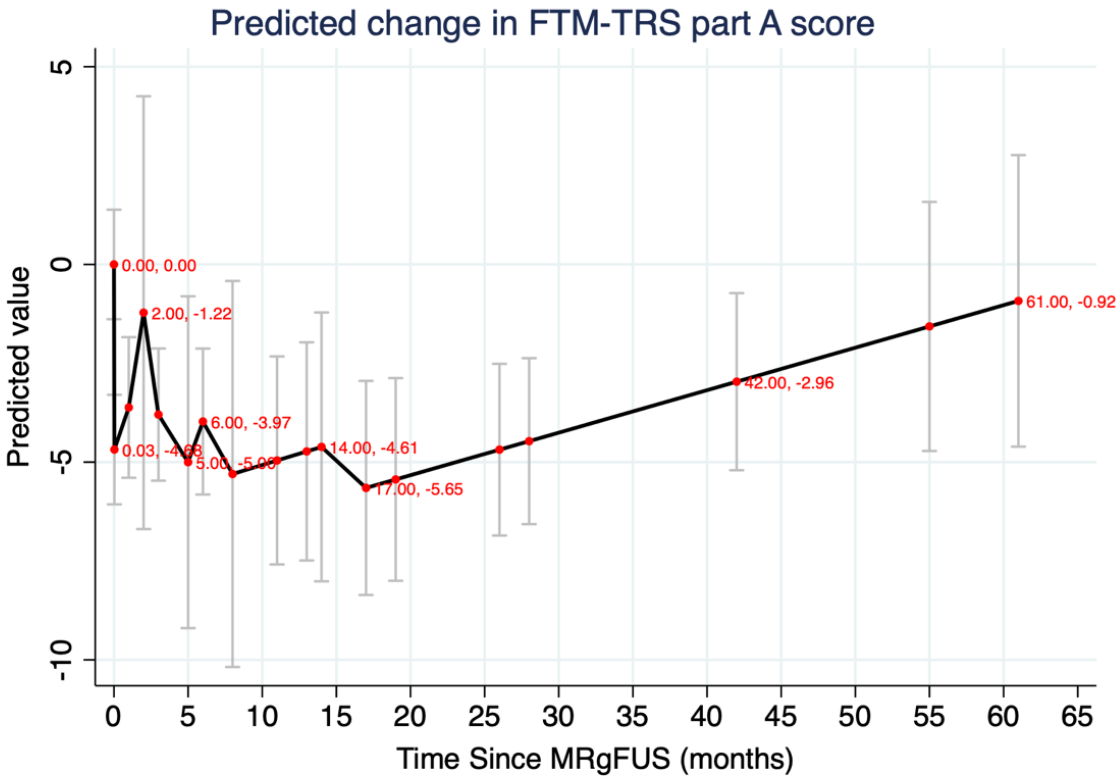

doi:10.6342/NTU202504209

Figure 3.1 Region mask editing with FSLeyes (Middle Cerebellar Peduncle)

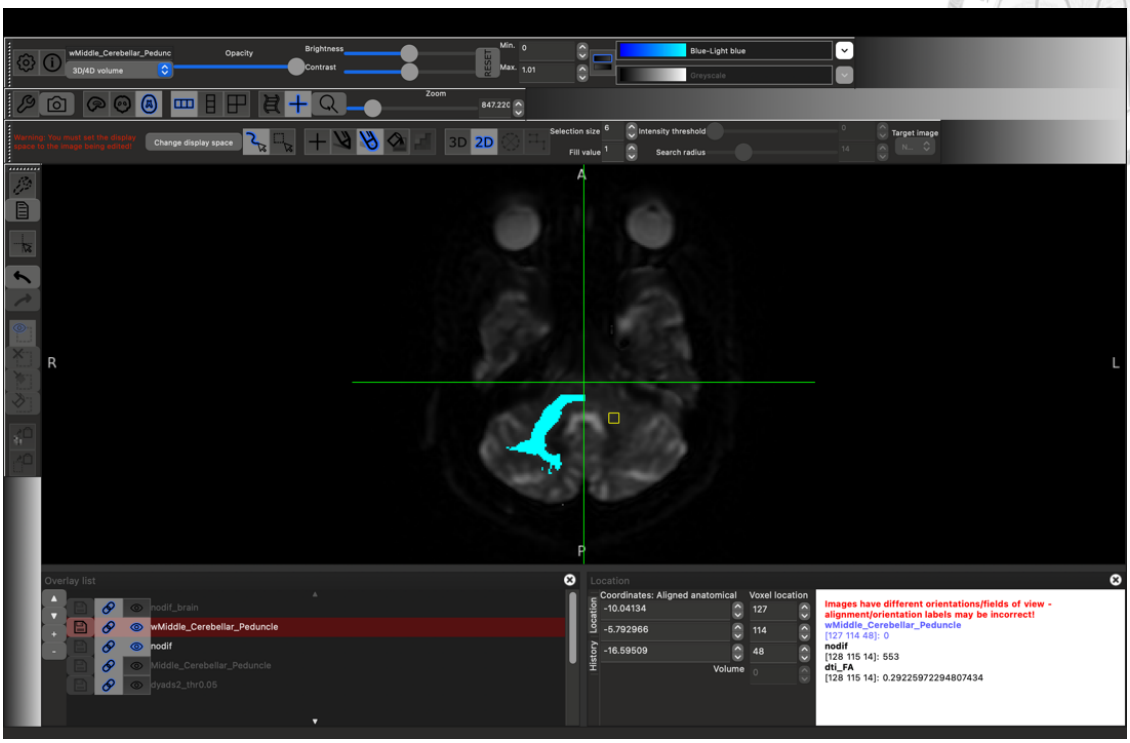

Figure 3.2.1 Region mask editing with FSLeyes (Superior Cerebellar Peduncle)

doi:10.6342/NTU202504209

Figure 3.2.2 Region mask editing with FSLeyes (Superior Cerebellar Peduncle)

doi:10.6342/NTU202504209

Figure 4. Contents of the TRS scale

Figure 4.1 TRS part A

Part A: Tremor Location/Severity Rating

	Rest	**Posture**	Action/ Intention	Total
1. Face tremor			XXXXXXXX	
2. Tongue tremor			XXXXXXXX	
3. Voice tremor	XXXX		XXXXXXXX	
4. Head tremor			XXXXXXXX	
5. RUE tremor				
6. LUE tremor				
7. Trunk tremor			XXXXXXXX	
8. RLE tremor				
9. LLE tremor				
10.Orthostaic (trunk/legs when standing)	XXXX		XXXXXXXX	

SUBTOTAL A: _____

1-10. **Tremor**: rate tremor
1. *At rest* (in repose), For head and trunk, when lying down.
2. *With posture holding* (UE-arms outstretched, wrists mildly extended, fingers spread apart; **LE-legs flexed at hips and knees), foot dorsiflexed; tongue-when protruded; head and trunk when sitting or standing.**
3. *With action and intention* (UE-finger to nose and other actions; LE-toe to finger in a flexed posture).

0 = None
1 = Slight; barely perceivable. May be intermittent.
2 = Moderate; amplitude <2 cm (extremities). May be intermittent.
3 = Marked; amplitude 2-4 cm (extremities).
4= Severe; amplitude > 4 cm (extremities).

doi:10.6342/NTU202504209

Figure 4.2 TRS part B

PART B: Specific Motor Tasks/Function Rating

	Right	Left	Total
11. Handwriting (dominant only)			
12. Drawing A:			
13. Drawing B:			
14. Drawing C:			
15. Pouring			

Subtotal Right : _____ Subtotal Left : _____ **SUBTOTAL B: _____**

11. **Handwriting:** Have a patient write the standard sentence "This is a sample of my best handwriting," sign his or her name, and write the date.
    - 0 = Normal
    - 1 = Mildly abnormal. Slightly untidy, tremulous
    - 2 = Moderately abnormal. Legible but with considerable tremor.
    - 3 = Markedly abnormal. Illegible.
    - 4 = Severely abnormal. Unable to keep pencil or pen on paper without holding hand down with the other hand

12-14. **Drawings (**See Figures A, B, and C below): Ask the patient to join both points of the various drawings without crossing the lines. Test each hand, beginning with the lesser involved without leaning the hand or arm on the table.
    - 0 = normal
    - 1 = Slightly tremulous. May cross lines occasionally.
    - 2 = Moderately tremulous or crosses lines frequently.
    - **3 = Accomplishes the task with great difficulty. Many errors.**
    - **4 = Unable to complete drawing.**

15. **Pouring**: Use firm plastic cups (8 cm tall), filled with water to 1 cm from top. Ask patient to pour water from one cup to another. Test each hand separately.
    - 0 = Normal
    - **1 = More careful than a person without tremor, but no water is spilled.**
    - 2 = Spills a small amount of water (up to 10% of total amount).
    - **3 = Spills a considerable amount of water (10-50%).**
    - 4 = Unable to pour without spilling most of the water.

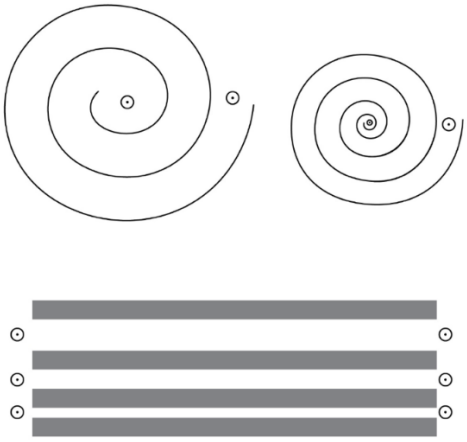

doi:10.6342/NTU202504209

Figure 4.3 TRS part C

Part C: Functional Disabilities Resulting from Tremor

Speaking	
Eating	
Drinking	
Hygiene	
Dressing	
Writing	
Working	
Social activities	

SUBTOTAL C: _____

TOTAL SCORE: _____

16. **Speaking:** This includes spastic dysphonia if present.
    0 = Normal
    1 = Mild voice tremulousness when nervous only.
    2 = Mild voice tremor, constant.
    3 = Moderate voice tremor.
    4 = Severe voice tremor. Some words difficult to understand.

17. **Feeding (**other than liquids):
    0 = Normal
    1 = Mildly abnormal. Can bring all solids to mouth, spilling only rarely.
    2 = Moderately abnormal. Frequent spills of peas and similar foods. May bring head at least halfway to meet food.
    3 = Marked abnormal. Unable to cut or uses two hands to feed.
    4 = Severely abnormal. Needs help to feed.

18. Bringing liquids to mouth:
    0 = Normal
    1 = Mildly abnormal. Can still use a spoon, but not if it is completely full.
    2 = Moderately abnormal. Unable to use a spoon. Uses cup or glass.
    3 = Markedly abnormal. Can drink from cup or glass, but needs two hands.
    4 = Severely abnormal. Must use a straw.

doi:10.6342/NTU202504209

Figure 5.1 Distribution of improvement rates in total tremor severity (TRS), treated hand (sel_Rt), and untreated hand (sel_Lt) during the early post-treatment phase. Percent improvement was calculated as (pre − post)/pre × 100%. Positive values indicate symptom improvement, while negative values indicate worsening.

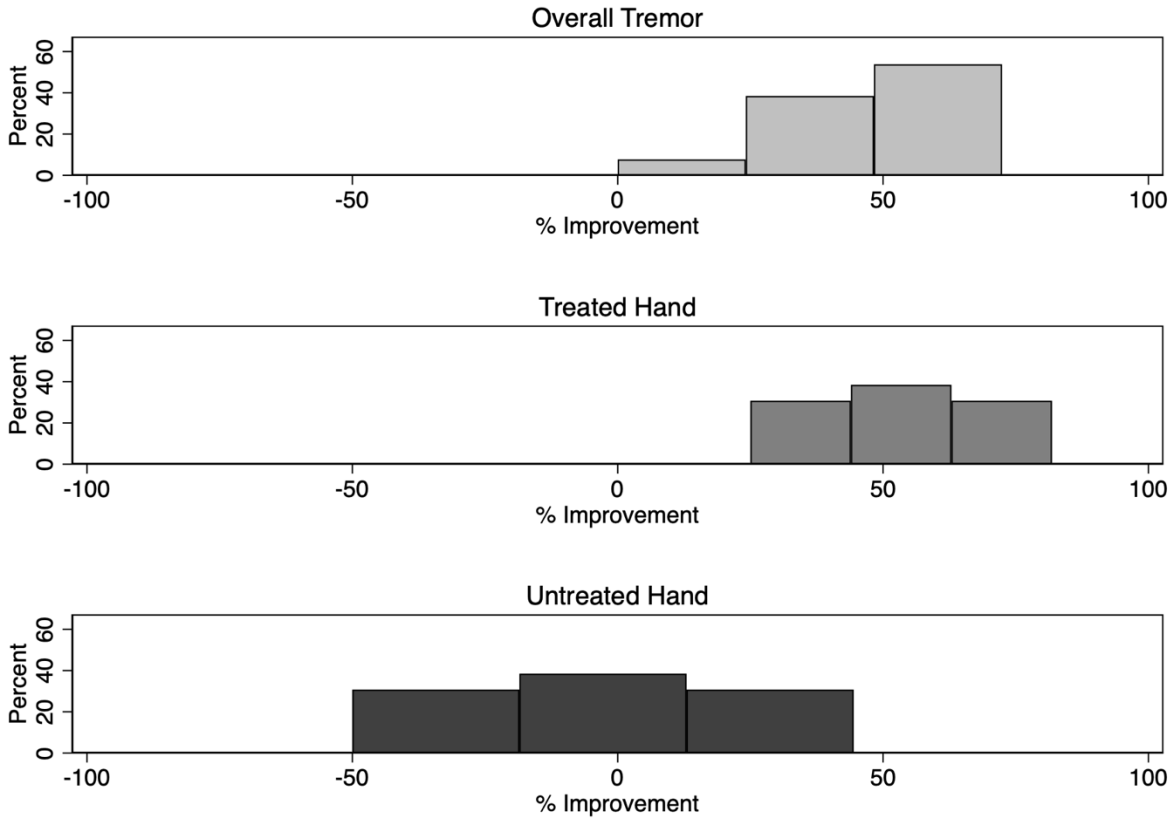

doi:10.6342/NTU202504209

Figure 5.2 Distribution of improvement rates in total tremor severity (TRS), treated hand (sel_Rt), and untreated hand (sel_Lt) during the late post-treatment phase. Percent improvement was calculated as (pre − post)/pre × 100%. Positive values indicate symptom improvement, while negative values indicate worsening.

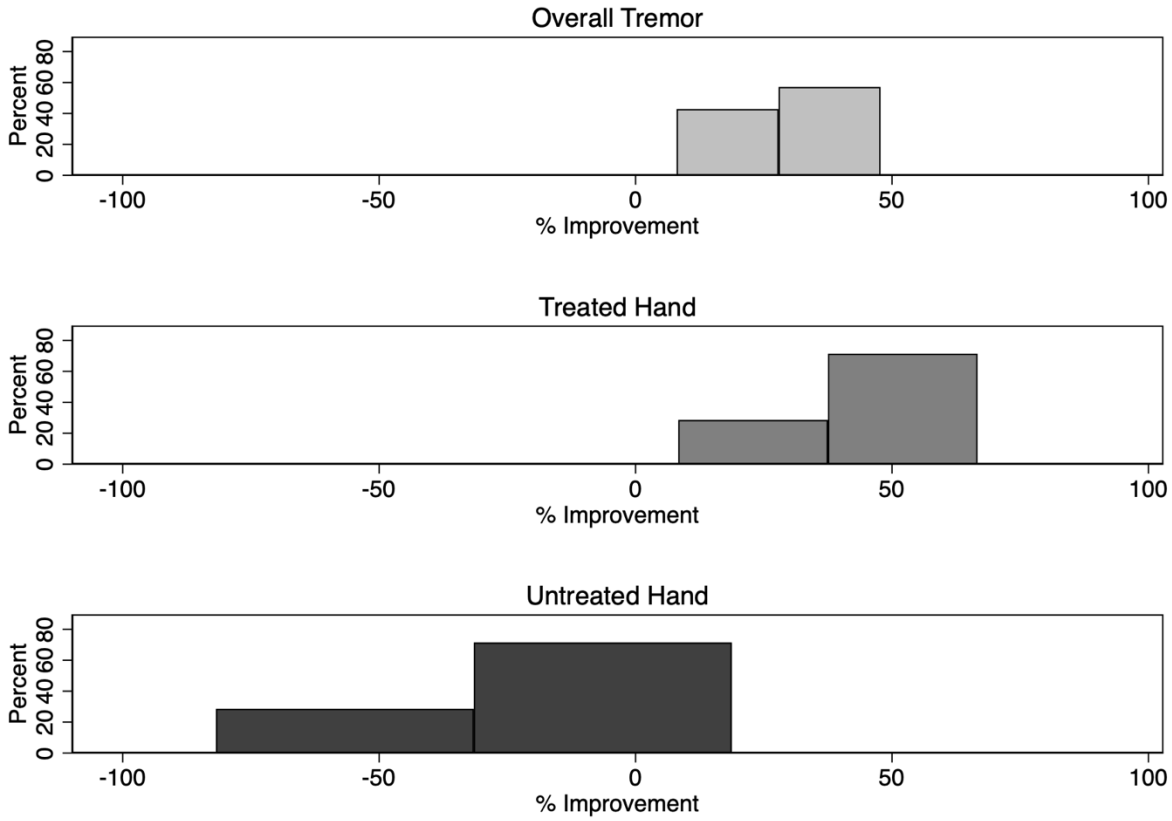

doi:10.6342/NTU202504209

Figure 6

Coefficient differences (Beta_Diff) between the sensitivity and original generalized estimating equation (GEE) models across all examined variables, plotted against the negative logarithm of the p-value ($-\log_{10}(p\_diff)$). Two variables exhibited statistically significant differences ($p\_diff < 0.05$) and are highlighted using distinct grayscale markers: a black square for *sel_Rt: TRS_category_num_4* and a dark gray diamond for *sel_Rtimproved: TRS_category_num_4*. These variables show substantial shifts in coefficient direction between models, consistent with the impact of excluding repeated second-side procedure data in the sensitivity analysis.

Note: *In the sensitivity model, data from ET001L and ET010R were excluded. To maintain balanced group sizes across time intervals, ET010R's follow-up MRI at 7 months post-treatment was categorized as part of TRS_category_num = 4 (i.e., the 4–6 month interval).*

doi:10.6342/NTU202504209

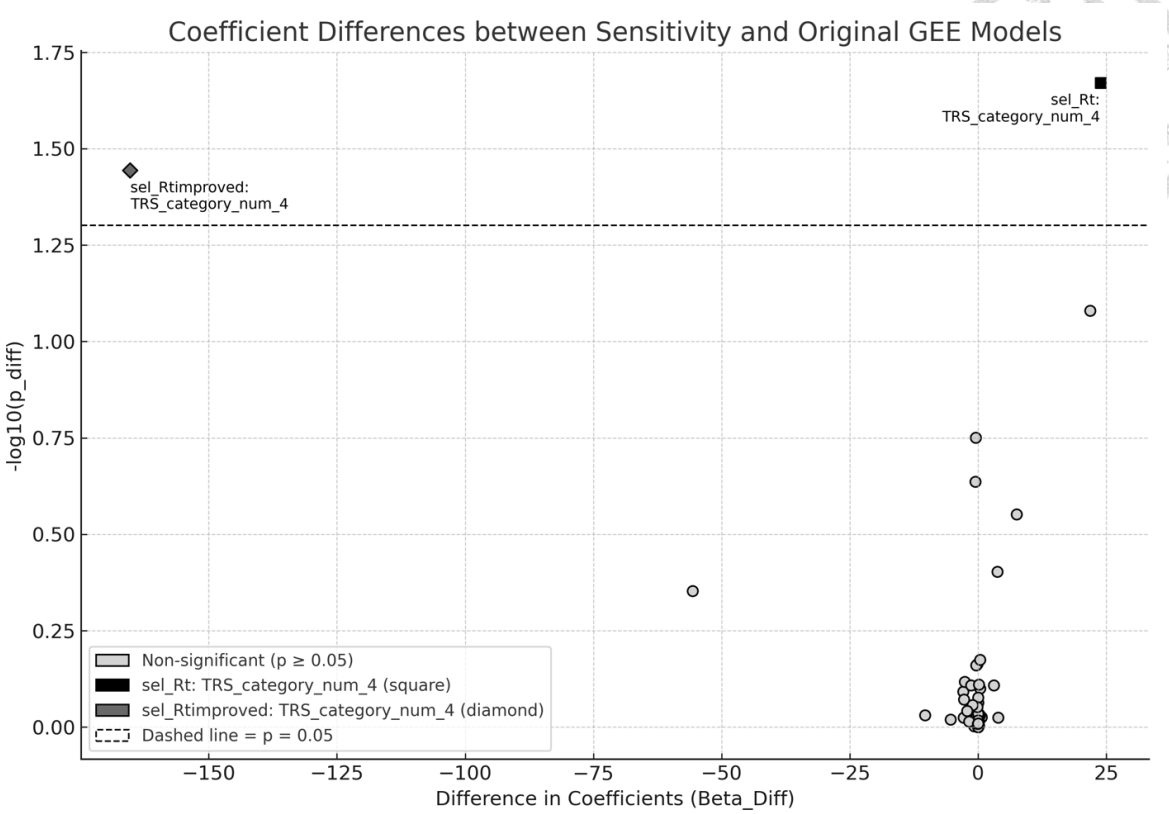

doi:10.6342/NTU202504209

Tables

Table 1. Main Cerebellar Input and Output Pathways

Table 1.1 Main Cerebellar Input Pathways

Deep Nuclei	Cerebellar Peduncle	Main Output Targets or Equivalent
Dentate Nucleus	Superior Cerebellar Peduncle	Ventrolateral nucleus of thalamus (VL), parvocellular red nucleus
Interposed Nuclei	Superior Cerebellar Peduncle	VL, magnocellular red nucleus
Fastigial Nuclei	Superior Cerebellar Peduncle	VL, tectum

Modified from (Lingford-Hughes & Kalk, 2012)

doi:10.6342/NTU202504209

Table 1.2 Main Cerebellar Output Pathways

Input Pathway	Main Origin(s) of Input	Cells Projecting to Cerebellum	Cerebellar Peduncle
Pontocerebellar fibers	Cortex	Pontine nuclei	Middle Cerebellar Peduncle
Spinocerebellar pathways			
Dorsal spinocerebellar tract	Leg proprioceptors	Nucleus dorsalis of Clark	Inferior Cerebellar Peduncle
Cuneocerebellar tract	Arm proprioceptors	External cuneate nucleus	Inferior Cerebellar Peduncle
Ventral spinocerebellar tract	Leg interneurons	Spinal cord neurons	Superior Cerebellar Peduncle
Rostral spinocerebellar tract	Arm interneurons	Spinal cord neurons	Superior & Inferior Cerebellar Peduncles
Climbing fibers	Red nucleus, cortex, brainstem, spinal cord	Inferior olivary nucleus	Inferior Cerebellar Peduncle

Modified from (Lingford-Hughes & Kalk, 2012)

doi:10.6342/NTU202504209

Table 2.1.1 The selection for each ROI (DTI)

	ROI	Importance
"Long tracts"	Corticospinal tract	Motion execution; possible implication in side-effects
	Frontopontine tract	Motion coordination; Tract lesion lead to ET tremor resolution
	Medial lemniscus	Possible implication in side-effects
	M1–Vim projection	Motion execution; Vim as lesioning target
Cerebellum	Motion execution; possible implication in side-effects Tract lesion lead to ET tremor resolution Possible implication in side-effects	Cerebellum conduits
Corpus Callosum	Corpus callosum- Genu Corpus callosum- Body Corpus callosum- Splenium Corpus callosum- Combined	Tremor worsened in untreated hand after MRgFUS thalamotomy

doi:10.6342/NTU202504209

Table 2.1.2 The selection rationale for each ROI (VBM)

	ROI	Importance
Cortex	Pre-supplementary motor area (preSMA) Supplementary motor area (SMA) Primary motor cortex (M1)	Cortical regions associated with motor planning, initiation, and execution
Thalamus	Ventral intermediate nucleus (Vim)	Lesion target; relay cerebellar output to motor cortical regions
	Ventral lateral posterior (VLp)	Encompasses Vim; relay cerebellar output to motor cortical regions
Cerebellum	Superior cerebellar peduncle (SCP) Middle cerebellar peduncle (MCP) Inferior cerebellar peduncle (ICP)	Cerebellar conduits
	Dorsal dentate nucleus	Major cerebellar output nucleus
Red Nucleus		Relay node within tremor network
Corpus Callosum	Corpus callosum- Genu Corpus callosum- Body Corpus callosum- Splenium Corpus callosum- Combined	Tremor worsened in untreated hand after MRgFUS thalamotomy

doi:10.6342/NTU202504209

Table 2.2.1 Summary of DTI Findings from Prior Cross-sectional Studies Comparing ET and HC

	ROI	Main Findings	References
"Long tracts"	Corticospinal tract	↑FA	(Gallea et al., 2015)
		↓FA, ↑MD	(Pietracupa et al., 2019)
	Corticospinal tract - L	FA↔, ↑MD	(Saini et al., 2012)
	Corticospinal tract - R	↑FA, MD ↔	(Saini et al., 2012)
	Frontopontine tract	-	
	Medial lemniscus	-	
	M1–Vim projection	FA ↔, ↓MD	(Revuelta et al., 2019)
Cerebellum	Superior cerebellar peduncle (SCP)	↓FA, ↑MD	(Nicoletti et al., 2010; Pietracupa et al., 2019; Tikoo et al., 2020)
	Superior cerebellar peduncle - L	↓FA	(Klein et al., 2011)
		↑FA, MD ↔	(Saini et al., 2012)

doi:10.6342/NTU202504209

Superior cerebellar peduncle - R	FA ↔, MD ↔	(Klein et al., 2011; Nicoletti et al., 2010)
Middle cerebellar peduncle (MCP)	FA ↔, MD ↔	(Nicoletti et al., 2010; Saini et al., 2012)
	↓FA, ↑MD	Pietracupa et al., 2019; Tikoo et al., 2020)
Middle cerebellar peduncle - L	FA ↔, MD ↔	(Klein et al., 2011)
Middle cerebellar peduncle - R	FA ↔, MD ↔	(Klein et al., 2011)
Inferior cerebellar peduncle (ICP)	↓FA, ↑MD	(Tikoo et al., 2020)
Inferior cerebellar peduncle (ICP)- L	FA ↔, ↑MD	(Klein et al., 2011)
	FA ↔, MD ↔	(Saini et al., 2012)
Inferior cerebellar peduncle (ICP)- R	↓FA, ↑MD	(Klein et al., 2011);
	FA ↔, MD ↔	(Nicoletti et al., 2010)

doi:10.6342/NTU202504209

Corpus Callosum	Corpus callosum- Genu	FA ↔, MD ↔	(Saini et al., 2012; Tantik Pak et al., 2021)
	Corpus callosum- Body	↓FA	(Tantik Pak et al., 2021)
	Corpus callosum- Splenium	FA ↔	(Tantik Pak et al., 2021)
	Corpus callosum- Combined	↓FA	(Prasad et al., 2018)

doi:10.6342/NTU202504209

Table 2.2.2 Summary of VBM Findings from Prior Cross-sectional Studies Comparing ET and HC

	ROI	Main Findings	References
Cortex	Pre-supplementary motor area (preSMA)	-	
	Supplementary motor area (SMA)	-	
	Primary motor cortex (M1)	↑	(Lin et al., 2013)
Thalamus	Ventral intermediate nucleus (Vim)	↓ bilateral thalamus	(Pietracupa et al., 2019)
	Ventral lateral posterior (VLp)	-	
Cerebellum	Superior cerebellar peduncle (SCP)	↔; ↓ R-SCP (ET + cerebellar s/sx)	(Prasad et al., 2019)
	Middle cerebellar peduncle (MCP)	↓	(Prasad et al., 2019)
	Inferior cerebellar peduncle (ICP)	↓	(Prasad et al., 2019)
	(Dorsal) dentate nucleus	↔	(Dyke et al., 2017)
	Red nucleus	↓	

doi:10.6342/NTU202504209

Corpus Callosum	Corpus callosum- Genu	-
	Corpus callosum – Body	
	Corpus callosum - Splenium	
	Corpus callosum - Combined	

doi:10.6342/NTU202504209

Table 2.3.1 Summary of Longitudinal DTI Changes in ET Patients Following MRgFUS Vim Thalamotomy: Evidence from Prior Studies

	ROI	Main Findings	References
"Long tracts"	Corticospinal tract	**(non-tx side)** no change at 3 months	(Pineda-Pardo et al., 2019)
		(tx side) ↓FA, ↔MD	(Thaler et al., 2023)
	Frontopontine tract	-	
	Medial lemniscus	**(non-tx side)** no change at 3 months	(Pineda-Pardo et al., 2019)
		(tx side) ↔FA, ↔MD	(Thaler et al., 2023)
	M1–Vim projection	-	
Cerebellum	Superior cerebellar peduncle (SCP) Middle cerebellar peduncle (MCP) Inferior cerebellar peduncle (ICP)	-	
Corpus Callosum	Corpus callosum- Genu Corpus callosum- Body Corpus callosum- Splenium	-	

doi:10.6342/NTU202504209

doi:10.6342/NTU202504209

Table 2.3.2 Summary of Longitudinal VBM Changes in ET Patients Following MRgFUS Vim Thalamotomy: Evidence from Prior Studies

	ROI	Main Findings	References
Cortex	Pre-supplementary motor area (preSMA)	-	
	Supplementary motor area (SMA)	-	
	Primary motor cortex (M1)	-	
Thalamus	Ventral intermediate nucleus (Vim)	↓ **at 6m** **No correlation with tremor reduction*	(Krauss et al., 2025)
	Ventral lateral posterior (VLp)	↓ **at 6m** **No correlation with tremor reduction*	(Krauss et al., 2025)
Cerebellum	Superior cerebellar peduncle (SCP)		
	Middle cerebellar peduncle (MCP)	-	
	Inferior cerebellar peduncle (ICP)		

doi:10.6342/NTU202504209

	(Dorsal) dentate nucleus	-
	Red nucleus	-
Corpus Callosum	Corpus callosum- Genu	-
	Corpus callosum – Body	
	Corpus callosum - Splenium	
	Corpus callosum - Combined	

doi:10.6342/NTU202504209

Table 3.1 Basic clinical information

Onset Age (year)		Disease Duration (year)		Age at surgery (year)		Family History of tremor	*N*
Min	13.2	Min	0.4	Min	20.2	+	17
Max	77.3	Max	40	Max	78.9	-	3
Mean	47.7	Mean	14.6	Mean	62.3		
SD	19.01	SD	12.41	SD	14.46		

doi:10.6342/NTU202504209

Table 3.2 Comorbidities

	N		*N*		*N*
Nil	5	Psychiatric disease	1	Asthma	1
Hypertension	5	Anemia	1	Hemorrhoids	1
Diabetes	2	Tumors	4	Cataract	1
Dyslipidemia	4	Fatty liver	1	Urticaria	1
Renal impairment	1	Inguinal hernia	1	Thyroid disease (thyroidectomy)	1

doi:10.6342/NTU202504209

Table 4 The distribution of baseline, early, and late MRI data and their corresponding intervals from the nearest TRS assessment.

Subject	MRI-early (months after surgery)	MRI-TRS interval (days)	MRI-late (months after surgery)	TRS-MRI interval (days)
ET001	6	0	17	0
ET002	6	3	61	0
ET003	6	20	NA	NA
ET004	NA	NA	55	0
ET005	NA	NA	NA	NA
ET006	NA	NA	17	0
ET007	NA	NA	42	0
ET008	7	17	NA	NA
ET009	NA	NA	NA	NA
ET010	7	0	28	40
ET010R	7	0	NA	NA
ET011	NA	NA	NA	NA
ET012	NA	NA	NA	NA
ET013	NA	NA	28	0
ET015	8	0	19	0
ET017R	7	0	NA	NA
ET018	6	0	NA	NA
ET019	9	0	NA	NA
ET020	7	0	NA	NA
PDET003	9	0	NA	NA
PDET004	10	0	NA	NA

doi:10.6342/NTU202504209

- **ET010R**: After undergoing left Vim thalamotomy, patient ET010 received a subsequent right Vim thalamotomy and was re-designated as ET010R.
- **ET017R**: A left-handed patient who underwent right Vim thalamotomy.
- **ET004**: MRgFUS treatment failed (unable to reach the therapeutic temperature); the patient subsequently underwent radiofrequency ablation thalamotomy, with follow-up MRI performed 55 months postoperatively.

doi:10.6342/NTU202504209

Table 5 Number of MRI datasets for ET at baseline, early, and late postoperative phases.

	Baseline	**Early**	**Late**
N	21	13 (12)	8

- After undergoing left Vim thalamotomy, ET010 subsequently received right Vim thalamotomy. This was counted as a separate case, resulting in a total of 21 baseline (preoperative) datasets. However, this particular dataset was excluded from the ET baseline vs. HC comparison.
- The MRI performed for ET015 during the ET-early phase was used exclusively for VBM analysis, as it did not contain the necessary data for DTI analysis.

doi:10.6342/NTU202504209

Table 6. Descriptive Statistics of Tremor Improvement: Early vs. Late Post-Treatment Stages

		TRS_%improved	sel_Rt%improved	sel_Lt%improved
Early post-treatement	mean	46.9	55.0	2.6
n=13	median	49.4	58.3	0.0
	SD	18.66	17.30	29.88
Late post-treatement	mean	32.8	41.6	-21.1
n=7	median	40.3	46.7	-5.0
	SD	15.22	19.98	38.99

**Improvement of TRS/ sel_Rt/ sel_Lt in percentage: (pre-post)/pre *100)*

doi:10.6342/NTU202504209

Table 7 Healthy Control Demographics

ALL HC	Mean Age	SD	Male	Female
n=23	59.7	18.1	13	10

- Two-sample T test with equal variances: p= 0.5238 (p >0.005); failed to reject H0

  There was no significant difference of age when HC and ET groups are compared

  (p = 0.5238)

doi:10.6342/NTU202504209

Table 8.1: GEE Model Results – FTM-TRS Part A Change (Post-MRgFUS – Baseline) vs. Time

TRSA change	Coef.	St.Err.	t-value	p-value	[95% Conf	Interval]	Sig
Timeintervalm_ad	.108	.057	1.90	.058	-.004	.219	*
TRS_category_num	0	.	.	.	.	.	
1	-4.685	.725	-6.46	0	-6.107	-3.264	***
2	-3.724	.923	-4.04	0	-5.533	-1.915	***
3	3.937	8.443	0.47	.641	-12.61	20.485	
4	-10.14	11.599	-0.87	.382	-32.873	12.594	
5	-6.214	6.736	-0.92	.356	-19.416	6.988	
6	-7.48	2.154	-3.47	.001	-11.701	-3.258	***
TRS_category_num#Timeintervalm_ad	0	.	.	.	.	.	
1†	0	.	.	.	.	.	
2†	0	.	.	.	.	.	
3	-2.686	2.867	-0.94	.349	-8.306	2.934	
4	.92	1.928	0.48	.633	-2.859	4.7	
5	.007	.556	0.01	.99	-1.083	1.096	
6†	0	.	.	.	.	.	
time_sq	-.007	.005	-1.21	.228	-.017	.004	
Constant	0	.707	0.00	1	-1.385	1.385	

Mean dependent var	-3.000	SD dependent var	3.852
Number of obs	92	Chi-square	55.706

*** *p*<.01, ** *p*<.05, * *p*<.1 †omitted due to collinearity

doi:10.6342/NTU202504209

Timeintervalm_ad= Time since MRgFUS (month)

TRS_category_num= Category of time interval since MRgFUS (0: baseline, 1: 1 day, 2: 1 month, 3: 2-3 months, 4: 4-6 months, 5: 7-14 months, 6: 15 months and up)

TRS_category_num#Timeintervalm_ad: interaction term between the categorical variable TRS_category_num and the continuous variable Timeintervalm_ad

doi:10.6342/NTU202504209

Table 8.2 GEE Model Results – Treated Hand FTM-TRS (Selected Items) vs. Time

sel_Rt	Coef.	St.Err.	t-value	p-value	[95% Conf	Interval]	Sig
Timeintervalm_ad	.739	.268	2.76	.006	.214	1.265	***
TRS_category_num	0	.	.	.	.	.	
1	-8.709	.446	-19.52	0	-9.583	-7.834	***
2	-8.292	.638	-12.99	0	-9.543	-7.041	***
3	-7.343	5.277	-1.39	.164	-17.686	3.001	
4	12.532	10.277	1.22	.223	-7.611	32.676	
5	-9.128	4.191	-2.18	.029	-17.343	-.914	**
6	-17.454	4.285	-4.07	0	-25.853	-9.056	***
TRS_category_num#Timeintervalm_ad	0	.	.	.	.	.	
1†	0	.	.	.	.	.	
2†	0	.	.	.	.	.	
3	-.578	1.812	-0.32	.75	-4.129	2.974	
4	-3.898	1.755	-2.22	.026	-7.338	-.458	**
5	-.468	.396	-1.18	.238	-1.245	.309	
6†	0	.	.	.	.	.	
sel_Lt_c	.477	.102	4.68	0	.277	.676	***
sel_Lt_c#Timeintervalm_ad	-.002	.005	-0.36	.72	-.013	.009	
TRS_category_num#c.sel_Lt_c	0	.	.	.	.	.	
1	-.324	.091	-3.57	0	-.502	-.146	***
2	-.144	.117	-1.23	.22	-.373	.086	
3	-.174	.105	-1.67	.095	-.379	.031	*
4	-.278	.12	-2.32	.02	-.513	-.043	**
5	-.337	.17	-1.98	.047	-.671	-.004	**
6	.026	.24	0.11	.915	-.444	.495	
time_sq	-.01	.004	-2.81	.005	-.017	-.003	***
Constant	13.717	.623	22.01	0	12.495	14.938	***

Mean dependent var	7.789	SD dependent var	4.531
Number of obs	90	Chi-square	475.132

*** *p<.01,* ** *p<.05,* * *p<.1* †omitted due to collinearity

doi:10.6342/NTU202504209

sel_Rt = Summation of specific items (rest, posture and action/intention tremor from TRS part A item 5, TRS part B item 12~14 of the treated hand) addressing tremor severity of the treated hand

Timeintervalm_ad= Time since MRgFUS (month)

TRS_category_num= Category of time interval since MRgFUS (0: baseline, 1: 1 day, 2: 1 month, 3: 2-3 months, 4: 4-6 months, 5: 7-14 months, 6: 15 months and up)

TRS_category_num#Timeintervalm_ad: interaction term between the categorical variable TRS_category_num and the continuous variable Timeintervalm_ad

sel_Lt_c: the mean-centered version of sel_Lt, the summation of specific items (rest, posture and action/intention tremor from TRS part A item 6, TRS part B item 12~14 of the non-treated hand) addressing tremor severity of the non-treated hand

sel_Lt_c# Timeintervalm_ad: interaction term between the categorical variable TRS_category_num and the continuous, centered variable sel_Lt_c

TRS_category_num#c.sel_Lt_c: interaction term between the categorical variable TRS_category_num and the continuous, centered variable sel_Lt_c

time_sq: the squared term of the variable Timeintervalm_ad

doi:10.6342/NTU202504209

Table 8.3: GEE Model Results – FTM-TRS (Selected Items) Change in the Treated Hand vs. Time

Change = Post-MRgFUS – Baseline

sel_Rt_num_change	Coef.	St.Err.	t-value	p-value	[95% Conf	Interval]	Sig
Timeintervalm_ad	.587	.312	1.88	.06	-.024	1.198	*
TRS_category_num	0	.	.	.	.	.	
1	-8.424	.562	-14.99	0	-9.525	-7.323	***
2	-7.626	.772	-9.88	0	-9.139	-6.114	***
3	-8.368	6.251	-1.34	.181	-20.619	3.882	
4	11.386	12.458	0.91	.361	-13.032	35.804	
5	-10.063	5.066	-1.99	.047	-19.993	-.134	**
6	-15.209	4.966	-3.06	.002	-24.943	-5.476	***
TRS_category_num#Timeintervalm_ad	0	.	.	.	.	.	
1†	0	.	.	.	.	.	
2†	0	.	.	.	.	.	
3	.058	2.143	0.03	.978	-4.142	4.258	
4	-3.582	2.127	-1.68	.092	-7.75	.586	*
5	-.302	.475	-0.64	.525	-1.233	.629	
6†	0	.	.	.	.	.	
sel_Lt_c	-.036	.067	-0.53	.594	-.168	.096	
time_sq	-.007	.004	-1.78	.074	-.015	.001	*
Constant	-.018	.501	-0.04	.971	-1	.964	
Mean dependent var		-5.444	SD dependent var			3.955	
Number of obs		90	Chi-square			273.520	

*** *p*<.01, ** *p*<.05, * *p*<.1 †omitted due to collinearity

sel_Rt_num_change = Change (post-MRgFUS – baseline) in total score from the specific items in FTM (rest, posture and action/intention tremor from TRS part A item 5, TRS part B item 12~14 of the treated hand)

Timeintervalm_ad= Time since MRgFUS (month)

doi:10.6342/NTU202504209

TRS_category_num= Category of time interval since MRgFUS (0: baseline, 1: 1 day, 2: 1 month, 3: 2-3 months, 4: 4-6 months, 5: 7-14 months, 6: 15 months and up)

TRS_category_num#Timeintervalm_ad: interaction term between the categorical variable TRS_category_num and the continuous variable Timeintervalm_ad

sel_Lt_c: the mean-centered version of sel_Lt, the summation of specific items (rest, posture and action/intention tremor from TRS part A item 6, TRS part B item 12~14 of the non-treated hand) addressing tremor severity of the non-treated hand

time_sq: the squared term of the variable Timeintervalm_ad

doi:10.6342/NTU202504209

Table 9.1 Sensitivity Analysis – FTM-TRS Part A Change (Post-MRgFUS – Baseline) vs. Time (Excluding Second-Side Procedures)

GEE model result- sensitivity analysis (full, includes time_sq)

TRSA_change	Coef.	St.Err.	t-value	p-value	[95% Conf	Interval]	Sig
Timeintervalm_ad	.61	.415	1.47	.141	-.203	1.423	
TRS_category_num	0	.	.	.	.	.	
1	-4.268	.759	-5.63	0	-5.755	-2.781	***
2	-4.086	1.031	-3.96	0	-6.106	-2.066	***
3	3.779	8.387	0.45	.652	-12.661	20.218	
4	-7.26	2.55	-2.85	.004	-12.258	-2.262	***
5	-6.902	6.723	-1.03	.305	-20.079	6.274	
6	-14.982	6.608	-2.27	.023	-27.933	-2.031	**
TRS_category_num# Timeintervalm_ad	0	.	.	.	.	.	
1†	0	.	.	.	.	.	
2†	0	.	.	.	.	.	
3	-3.025	2.879	-1.05	.294	-8.668	2.619	
4†	0	.	.	.	.	.	
5	-.353	.63	-0.56	.576	-1.589	.883	
6†	0	.	.	.	.	.	
time_sq	-.007	.005	-1.22	.222	-.017	.004	
Constant	0	.719	-0.00	1	-1.409	1.409	
Mean dependent var		-2.812	SD dependent var			3.740	
Number of obs		85	Chi-square			46.391	

*** *p<.01,* ** *p<.05,* * *p<.1* †omitted due to collinearity

Timeintervalm_ad= Time since MRgFUS (month)

TRS_category_num= Category of time interval since MRgFUS (0: baseline, 1: 1 day, 2: 1 month, 3: 2-3 months, 4: 4-6 months, 5: 7-14 months, 6: 15 months and up)

TRS_category_num#Timeintervalm_ad: interaction term between the categorical variable TRS_category_num and the continuous variable Timeintervalm_ad

doi:10.6342/NTU202504209

time_sq: the squared term of the variable Timeintervalm_ad

doi:10.6342/NTU202504209

Table 9.2 Sensitivity Analysis – Treated Hand FTM-TRS (Selected Items) vs. Time

(Excluding Second-Side Procedures)

GEE model result-sensitivity analysis

sel_Rt	Coef.	St.Err.	t-value	p-value	[95% Conf	Interval]	Sig
Timeintervalm_ad	.753	.237	3.17	.002	.287	1.218	***
TRS_category_num	0	.	.	.	.	.	
1	-8.678	.419	-20.72	0	-9.499	-7.857	***
2	-8.322	.575	-14.48	0	-9.448	-7.195	***
3	-6.904	4.648	-1.49	.137	-16.014	2.206	
4	-11.351	1.444	-7.86	0	-14.181	-8.521	***
5	-8.897	3.705	-2.40	.016	-16.158	-1.636	**
6	-17.515	3.792	-4.62	0	-24.946	-10.084	***
TRS_category_num# Timeintervalm_ad	0	.	.	.	.	.	
1†	0	.	.	.	.	.	
2†	0	.	.	.	.	.	
3	-.799	1.598	-0.50	.617	-3.932	2.334	
4†	0	.	.	.	.	.	
5	-.499	.351	-1.42	.155	-1.186	.188	
6†	0	.	.	.	.	.	
sel_Lt_c	.5	.086	5.80	0	.331	.669	***
sel_Lt_c# Timeintervalm_ad	-.002	.005	-0.33	.743	-.011	.008	
TRS_category_num# c.sel_Lt_c	0	.	.	.	.	.	
1	-.345	.082	-4.23	0	-.505	-.185	***
2	-.16	.104	-1.54	.125	-.364	.044	
3	-.176	.094	-1.88	.06	-.359	.008	*
4	-.245	.108	-2.27	.023	-.457	-.034	**
5	-.359	.151	-2.38	.017	-.655	-.063	**
6	-.005	.213	-0.02	.981	-.422	.412	
time_sq	-.01	.003	-3.25	.001	-.016	-.004	***
Constant	13.25	.508	26.07	0	12.254	14.247	***

Mean dependent var	7.253	SD dependent var	4.126
Number of obs	83	Chi-square	553.478

*** *p*<.01, ** *p*<.05, * *p*<.1 †omitted due to collinearity

doi:10.6342/NTU202504209

sel_Rt = Summation of specific items (rest, posture and action/intention tremor from TRS part A item 5, TRS part B item 12~14 of the treated hand) addressing tremor severity of the treated hand

Timeintervalm_ad= Time since MRgFUS (month)

TRS_category_num= Category of time interval since MRgFUS (0: baseline, 1: 1 day, 2: 1 month, 3: 2-3 months, 4: 4-6 months, 5: 7-14 months, 6: 15 months and up)

TRS_category_num#Timeintervalm_ad: interaction term between the categorical variable TRS_category_num and the continuous variable Timeintervalm_ad

sel_Lt_c: the mean-centered version of sel_Lt, the summation of specific items (rest, posture and action/intention tremor from TRS part A item 6, TRS part B item 12~14 of the non-treated hand) addressing tremor severity of the non-treated hand

sel_Lt_c# Timeintervalm_ad: interaction term between the categorical variable TRS_category_num and the continuous, centered variable sel_Lt_c

TRS_category_num#c.sel_Lt_c: interaction term between the categorical variable TRS_category_num and the continuous, centered variable sel_Lt_c

time_sq: the squared term of the variable Timeintervalm_ad

doi:10.6342/NTU202504209

Table 9.3 Sensitivity Analysis – FTM-TRS (Selected Items) Change in the Treated Hand vs. Time (Excluding Second-Side Procedures)

Change = Post-MRgFUS – Baseline

GEE model result-sensitivity analysis

sel_Rt_num_change	Coef.	St.Err.	t-value	p-value	[95% Conf	Interval]	Sig
Timeintervalm_ad	.592	.319	1.86	.063	-.033	1.218	*
TRS_category_num	0	.	.	.	.	.	
1	-8.307	.605	-13.73	0	-9.494	-7.121	***
2	-7.655	.799	-9.59	0	-9.22	-6.089	***
3	-8.097	6.417	-1.26	.207	-20.674	4.48	
4	-10.469	1.963	-5.33	0	-14.316	-6.623	***
5	-9.885	5.191	-1.90	.057	-20.06	.289	*
6	-15.279	5.087	-3.00	.003	-25.25	-5.308	***
TRS_category_num# Timeintervalm_ad	0	.	.	.	.	.	
1†	0	.	.	.	.	.	
2†	0	.	.	.	.	.	
3	-.07	2.203	-0.03	.975	-4.388	4.249	
4†	0	.	.	.	.	.	
5	-.322	.486	-0.66	.508	-1.275	.632	
6†	0	.	.	.	.	.	
sel_Lt_c	-.031	.071	-0.44	.66	-.17	.108	
time_sq	-.007	.004	-1.76	.078	-.015	.001	*
Constant	-.019	.544	-0.03	.972	-1.086	1.048	
Mean dependent var		-5.506	SD dependent var			3.974	
Number of obs		83	Chi-square			237.298	

*** *p<.01,* ** *p<.05,* * *p<.1* †omitted due to collinearity

sel_Rt_num_change = Change (post-MRgFUS – baseline) in total score from the specific items in FTM (rest, posture and action/intention tremor from TRS part A item 5, TRS

doi:10.6342/NTU202504209

part B item 12~14 of the treated hand)

Timeintervalm_ad= Time since MRgFUS (month)

TRS_category_num= Category of time interval since MRgFUS (0: baseline, 1: 1 day, 2: 1 month, 3: 2-3 months, 4: 4-6 months, 5: 7-14 months, 6: 15 months and up)

TRS_category_num#Timeintervalm_ad: interaction term between the categorical variable TRS_category_num and the continuous variable Timeintervalm_ad

sel_Lt_c: the mean-centered version of sel_Lt, the summation of specific items (rest, posture and action/intention tremor from TRS part A item 6, TRS part B item 12~14 of the non-treated hand) addressing tremor severity of the non-treated hand

time_sq: the squared term of the variable Timeintervalm_ad

doi:10.6342/NTU202504209

Table 10.1 DTI Regression summary: ET vs. HC by Region (Dominant hand)

Adjusted for age, sex and TRS total score

Regression summary: ET vs. HC by Region (Dominant hand)

Region	FA_Coef	FA_pval	FA_p_raw	FA_p_FDR	MD_Coef	MD_pval	MD_p_raw	MD_p_FDR
L_Corticospinal_Tract	-0.014	0.2224	0.222	0.445	0.015	0.6789	0.679	1
L_Frontopontine_Tract	-0.019	0.1314	0.131	0.350	0.053	0.2109	0.211	0.562
L_Medial_Lemniscus	0.016	0.3929	0.393	0.524	-0.005	0.8605	0.860	0.983
L_M1Vim	-0.019	0.3136	0.314	0.502	-0.008	0.7929	0.793	1
R_SCP	0.008	0.6600	0.660	0.754	0.004	0.9474	0.947	0.947
R_MCP	0.030	0.0187*	0.019	0.075	0.010	0.5643	0.564	1
R_ICP_HCP482	0.037	0.0170*	0.017	0.136	-0.058	0.1443	0.144	0.577
R_ICP_JHU	0.008	0.6924	0.692	0.692	-0.107	0.0569	0.057	0.455

*** $p < 0.001$, ** $p < 0.01$, * $p < 0.05$

doi:10.6342/NTU202504209

Table 10.2 DTI Regression summary: ET vs. HC by Region (Non-dominant hand)

Adjusted for age, sex and TRS total score

Regression summary: ET vs. HC by Region (Non-dominant hand)

Region	FA_Coef	FA_pval	FA_p_raw	FA_p_FDR	MD_Coef	MD_pval	MD_p_raw	MD_p_FDR
R_Corticospinal_Tract	-0.020	0.0878	0.088	0.702	0.033	0.2710	0.271	0.723
R_Frontopontine_Tract	-0.014	0.2050	0.205	0.820	0.052	0.3340	0.334	0.668
R_Medial_Lemniscus	0.016	0.3836	0.384	0.767	-0.022	0.5727	0.573	0.655
R_M1Vim	-0.011	0.5370	0.537	0.716	0.026	0.3822	0.382	0.612
L_SCP	0.017	0.4015	0.401	0.642	-0.061	0.2129	0.213	0.852
L_MCP	0.004	0.7805	0.780	0.780	0.004	0.8277	0.828	0.828
L_ICP_HCP482	0.020	0.2378	0.238	0.634	-0.054	0.1101	0.110	0.881
L_ICP_JHU	0.006	0.7742	0.774	0.885	-0.034	0.4723	0.472	0.630

*** $p < 0.001$, ** $p < 0.01$, * $p < 0.05$

doi:10.6342/NTU202504209

Table 10.3 DTI Regression summary: ET-late vs. HC by Region (Corpus Callosum)

Adjusted for age, sex and TRS total score

Regression summary: ET vs. HC by Region (Corpus Callosum)

Region	FA_Coef	FA_pval	MD_Coef	MD_pval
Corpus_Callosum_Genu	0.012	0.6665	0.021	0.8399
Corpus_Callosum_Body	-0.002	0.9535	-0.067	0.3549
Corpus_Callosum_Splenium	0.003	0.9054	-0.039	0.6496
Corpus_Callosum_Combined	0.002	0.9322	-0.026	0.7287

*** $p < 0.001$, ** $p < 0.01$, * $p < 0.05$

doi:10.6342/NTU202504209

Table 11.1 VBM ET vs. HC (Dominant Hand)

Adjusted for age, sex and TRS total score

Region	Coef	Pval_combined
L_preSMA	0.063	0.1007
L_SMA	-0.054	0.2265
L_M1	0.039	0.2357
L_VIM	-0.067	0.2754
L_VLp	-0.053	0.3754
R_Dorsal_Dentate_Nucleus	-0.005	0.7424
L_Red_Nucleus	-0.002	0.6518
TRS	-0.000	.

Region	Coef	Pval_combined
R_SCP	0.097	0.0766
R_MCP	0.096	0.0400*
	0.105	0.0256*
R_ICP_HCP 482		
R_ICP_JHU	0.082	0.1319
TRS	-0.000	.

doi:10.6342/NTU202504209

Table 11.2 VBM ET vs. HC (Non-dominant Hand)

Adjusted for age, sex and TRS total score

Region	Coef	Pval_combined
R_preSMA	0.060	0.1258
R_SMA	0.053	0.4201
R_M1	-0.002	0.9341
R_VIM	-0.060	0.2756
R_VLp	-0.067	0.2167
L_Dorsal_Dentate_Nucleus	0.021	0.1174
R_Red_Nucleus	0.004	0.1983
TRS	-0.000	.

Region	Coef	Pval_combined
L_SCP	0.096	0.0849
L_MCP	0.090	0.0583
	0.105	0.0244*
L_ICP_HCP 482		
L_ICP_JHU	0.091	0.0968
TRS	-0.000	.

doi:10.6342/NTU202504209

Table 11.3 VBM ET vs. HC (Corpus callosum)

Adjusted for age, sex and TRS total score

Region	Coef	Pval_combined
Corpus_Callosum_Genu	0.068	0.2335
Corpus_Callosum_Body	0.059	0.2606
Corpus_Callosum_Splenium	0.077	0.2130
Corpus_Callosum_Combined	0.068	0.2189
TRS	-0.000	.

doi:10.6342/NTU202504209

Table 12.1 DTI Regression summary: ET-early vs. HC by Region (Treated hand)

Adjusted for age, sex and TRS total score

Region	FA_Coef	FA_pval	FA_p_raw	FA_p_FDR	MD_Coef	MD_pval	MD_p_raw	MD_p_FDR
L_Corticospinal_Tract	-0.054	0.0559	0.056	0.126	0.085	0.2827	0.283	0.509
L_Frontopontine_Tract	-0.062	0.1306	0.131	0.168	0.150	0.0795	0.079	0.715
L_Medial_Lemniscus	0.096	0.0369*	0.037	0.111	0.147	0.1164	0.116	0.524
L_M1Vim	-0.089	0.0909	0.091	0.164	0.117	0.1722	0.172	0.517
R_SCP	0.122	0.0337*	0.034	0.152	-0.131	0.3834	0.383	0.575
R_MCP	0.045	0.1780	0.178	0.200	0.013	0.8311	0.831	0.935
R_ICP_HCP482	0.095	0.0217*	0.022	0.195	-0.112	0.2356	0.236	0.530
R_ICP_JHU	0.045	0.4447	0.445	0.445	-0.049	0.7541	0.754	0.970
MRI_time (covariate)	0.005	0.1224	0.122	0.184	.	.	.	1

*** $p < 0.001$, ** $p < 0.01$, * $p < 0.05$

doi:10.6342/NTU202504209

Table 12.2 DTI Regression summary: ET-early vs. HC by Region (Non-treated hand)

Adjusted for age, sex and TRS total score

Region	FA_Coef	FA_pval	FA_p_raw	FA_p_FDR	MD_Coef	MD_pval	MD_p_raw	MD_p_FDR
R_Corticospinal_Tract	0.019	0.5239	0.524	0.674	0.119	0.0578	0.058	0.260
R_Frontopontine_Tract	0.029	0.4852	0.485	0.728	0.226	0.0558	0.056	0.502
R_Medial_Lemniscus	0.131	0.0031**	0.003	0.028*	-0.049	0.6658	0.666	1
R_M1Vim	0.058	0.3512	0.351	0.632	-0.017	0.8331	0.833	1
L_SCP	0.125	0.0243*	0.024	0.109	-0.158	0.2532	0.253	0.760
L_MCP	0.065	0.0480*	0.048	0.144	0.010	0.8650	0.865	0.973
L_ICP_HCP482	0.051	0.2501	0.250	0.563	-0.033	0.7328	0.733	1
L_ICP_JHU	-0.013	0.8309	0.831	0.831	0.037	0.7922	0.792	1
MRI_time (covariate)	-0.002	0.6010	0.601	0.676	.	.	.	1

*** $p < 0.001$, ** $p < 0.01$, * $p < 0.05$

doi:10.6342/NTU202504209

Table 12.3 DTI Regression summary: ET-early vs. HC by Region (Corpus Callosum)

Adjusted for age, sex and TRS total score

Region	FA_Coef	FA_pval	MD_Coef	MD_pval
Corpus_Callosum_Genu	0.154	0.0330*	-0.145	0.6263
Corpus_Callosum_Body	0.125	0.0495*	-0.177	0.2069
Corpus_Callosum_Splenium	0.178	0.0243*	-0.560	0.0211*
Corpus_Callosum_Combined	0.152	0.0197*	-0.316	0.1280
MRI_time (covariate)	-0.016	0.0306*	0.028	0.2387

*** $p < 0.001$, ** $p < 0.01$, * $p < 0.05$

doi:10.6342/NTU202504209

Table 13.1 VBM ET-early vs. HC (Treated Hand)

Adjusted for age, sex and TRS total score

Region	Coef	Pval_combined
L_preSMA	0.068	0.0592
L_SMA	-0.036	0.4070
L_M1	0.022	0.5486
L_VIM	-0.013	0.7710
L_VLp	0.009	0.8462
R_Dorsal_Dentate_Nucleus	-0.035	0.0252*
L_Red_Nucleus	0.001	0.8003
TRS	-0.000	.

*** $p < 0.001$, ** $p < 0.01$, * $p < 0.05$

Region	Coef	Pval_combined
R_SCP	0.040	0.4525
R_MCP	0.037	0.4254
R_ICP_HCP 482	0.028	0.5587
R_ICP_JHU	0.024	0.6678
TRS	-0.000	.

*** $p < 0.001$, ** $p < 0.01$, * $p < 0.05$

doi:10.6342/NTU202504209

Table 13.2 VBM ET-early vs. HC (Non-treated Hand)

Adjusted for age, sex and TRS total score

Region	Coef	Pval_combined
R_preSMA	0.078	0.0588
R_SMA	0.047	0.5002
R_M1	-0.014	0.7166
R_VIM	0.071	0.2078
R_VLp	0.051	0.3223
L_Dorsal_Dentate_Nucleus	0.041	0.0159*
R_Red_Nucleus	-0.001	0.7006
TRS	-0.000	.

*** $p < 0.001$, ** $p < 0.01$, * $p < 0.05$

Region	Coef	Pval_combined
L_SCP	0.020	0.7215
L_MCP	0.022	0.6396
L_ICP_HCP 482	0.001	0.9878
L_ICP_JHU	0.021	0.7104
TRS	-0.000	.

*** $p < 0.001$, ** $p < 0.01$, * $p < 0.05$

doi:10.6342/NTU202504209

Table 13.3 VBM ET-early vs. HC (Corpus callosum)

Adjusted for age, sex and TRS total score

Region	Coef	Pval_combined
Corpus_Callosum_Genu	0.045	0.3096
Corpus_Callosum_Body	0.046	0.3074
Corpus_Callosum_Splenium	0.069	0.2454
Corpus_Callosum_Combined	0.054	0.2677
TRS	-0.000	.

*** $p < 0.001$, ** $p < 0.01$, * $p < 0.05$

doi:10.6342/NTU202504209

Table 14.1 DTI Regression summary: ET-late vs. HC by Region (Treated hand)

Adjusted for age, sex and TRS total score

Region	FA_Coef	FA_pval	FA_p_raw	FA_p_FDR	MD_Coef	MD_pval	MD_p_raw	MD_p_FDR
L_Corticospinal_Tract	-0.030	0.1888	0.189	1	0.054	0.3430	0.343	1
L_Frontopontine_Tract	-0.015	0.5721	0.572	1	0.034	0.5996	0.600	1
L_Medial_Lemniscus	0.018	0.5765	0.576	1	-0.065	0.2266	0.227	1
L_M1Vim	-0.013	0.7376	0.738	0.902	0.009	0.8774	0.877	1
L_VApreSMA_subject_mask	0.001	0.9632	0.963	0.963	-0.022	0.7729	0.773	1
L_VASMA_subject_mask	-0.022	0.6107	0.611	1	-0.006	0.9512	0.951	1
R_SCP	-0.027	0.5444	0.544	1	0.018	0.8900	0.890	1
R_MCP	-0.008	0.7212	0.721	0.992	-0.001	0.9875	0.988	0.988
R_ICP_HCP482	-0.010	0.7180	0.718	1	-0.030	0.7086	0.709	1
R_ICP_JHU	-0.038	0.2485	0.249	1	-0.033	0.7903	0.790	1
MRI_time (covariate)	-0.000	0.9209	0.921	1	-0.001	0.4680	0.468	1

*** $p < 0.001$, ** $p < 0.01$, * $p < 0.05$

doi:10.6342/NTU202504209

Table 14.2 DTI Regression summary: ET-late vs. HC by Region (Non-treated hand)

Adjusted for age, sex and TRS total score

Region	FA_Coef	FA_pval	FA_p_raw	FA_p_FDR	MD_Coef	MD_pval	MD_p_raw	MD_p_FDR
R_Corticospinal_Tract	0.002	0.9264	0.926	0.926	0.001	0.9885	0.988	0.988
R_Frontopontine_Tract	0.003	0.8990	0.899	0.989	-0.002	0.9813	0.981	1
R_Medial_Lemniscus	0.019	0.6004	0.600	1	-0.071	0.3596	0.360	1
R_M1Vim	-0.026	0.5451	0.545	1	0.002	0.9660	0.966	1
R_VApreSMA_subject_mask	0.012	0.7334	0.733	1	-0.011	0.9159	0.916	1
R_VASMA_subject_mask	0.011	0.7681	0.768	0.939	-0.083	0.3367	0.337	1
L_SCP	-0.032	0.5149	0.515	1	-0.053	0.6383	0.638	1
L_MCP	-0.027	0.2919	0.292	1	-0.003	0.9364	0.936	1
L_ICP_HCP482	-0.023	0.5728	0.573	1	-0.020	0.7816	0.782	1
L_ICP_JHU	0.016	0.7171	0.717	1	-0.025	0.8134	0.813	1
MRI_time (covariate)	-0.001	0.0942	0.094	1	0.000	0.5936	0.594	1

*** $p < 0.001$, ** $p < 0.01$, * $p < 0.05$

doi:10.6342/NTU202504209

Table 14.3 DTI Regression summary: ET-late vs. HC by Region (Corpus Callosum)

Adjusted for age, sex and TRS total score

Region	FA_Coef	FA_pval	MD_Coef	MD_pval
Corpus_Callosum_Genu	0.004	0.9218	-0.012	0.9389
Corpus_Callosum_Body	-0.053	0.1660	0.083	0.2629
Corpus_Callosum_Splenium	-0.045	0.2155	0.078	0.4539
Corpus_Callosum_Combined	-0.035	0.3357	0.053	0.6049
MRI_time (covariate)	-0.001	0.2826	0.002	0.5074

doi:10.6342/NTU202504209

Table 15.1 VBM ET-late vs. HC (Treated Hand)

Adjusted for age, sex and TRS total score

Region	Coef	Pval_combined
L_preSMA	-0.021	0.6808
L_SMA	-0.046	0.4098
L_M1	-0.016	0.7038
L_VIM	-0.016	0.7857
L_VLp	-0.027	0.6374
R_Dorsal_Dentate_Nucleus	-0.008	0.7020
L_Red_Nucleus	-0.000	0.9421
TRS	0.000	.

Region	Coef	Pval_combined
R_SCP	0.066	0.3239
R_MCP	0.047	0.4335
R_ICP_HCP482	0.057	0.3214
R_ICP_JHU	0.053	0.4483
TRS	0.000	.

doi:10.6342/NTU202504209

Table 15.2 VBM ET-late vs. HC (Non-treated Hand)

Adjusted for age, sex and TRS total score

Region	Coef	Pval_combined
R_preSMA	-0.035	0.3553
R_SMA	-0.000	0.9979
R_M1	0.021	0.5749
R_VIM	-0.011	0.8516
R_VLp	-0.020	0.7113
L_Dorsal_Dentate_Nucleus	0.000	0.9948
R_Red_Nucleus	0.000	0.9057
TRS	0.000	.

Region	Coef	Pval_combined
L_SCP	0.053	0.4526
L_MCP	0.043	0.4898
	0.039	0.5159
L_ICP_HCP482		
L_ICP_JHU	0.057	0.4215
TRS	0.000	.

doi:10.6342/NTU202504209

Table 15.3 VBM ET-late vs. HC (Corpus callosum)

Adjusted for age, sex and TRS total score

Region	Coef	Pval_combined
Corpus_Callosum_Genu	0.070	0.2213
Corpus_Callosum_Body	0.049	0.3453
Corpus_Callosum_Splenium	0.078	0.2876
	0.065	0.2630
Corpus_Callosum_Combined		
TRS	0.000	.

doi:10.6342/NTU202504209

Table 16.1 Paired regression: DTI early vs baseline, clustered by subject (Treated hand)

Adjusted for age, sex and TRS total score

Region	FA_Coef	FA_pval	MD_Coef	MD_pval
L_Corticospinal_Tract	-0.001	1.0000	0.026	1.0000
L_Frontopontine_Tract	0.004	1.0000	0.008	1.0000
L_M1Vim	0.023	1.0000	0.017	0.9517
L_Medial_Lemniscus	-0.012	1.0000	0.034	1.0000
R_ICP_HCP482	-0.010	1.0000	0.032	1.0000
R_ICP_JHU	0.003	1.0000	0.066	0.8317
R_MCP	-0.007	0.9523	-0.001	0.9756
R_SCP	0.002	0.9812	0.034	1.0000

doi:10.6342/NTU202504209

Table 16.2 Paired regression: DTI early vs baseline, clustered by subject (Non-treated hand)

Adjusted for age, sex and TRS total score

Region	FA_Coef	FA_pval	MD_Coef	MD_pval
R_Corticospinal_Tract	0.006	0.9960	0.001	1.0000
R_Frontopontine_Tract	0.006	0.9732	-0.014	1.0000
R_Medial_Lemniscus	-0.001	1.0000	0.027	1.0000
R_M1Vim	-0.008	1.0000	0.027	1.0000
L_SCP	-0.018	1.0000	0.059	1.0000
L_MCP	-0.000	1.0000	0.006	1.0000
L_ICP_HCP482	0.000	0.9781	0.019	0.9162
L_ICP_JHU	0.021	1.0000	-0.028	1.0000

doi:10.6342/NTU202504209

Table 16.3 Paired regression: DTI early vs baseline, clustered by subject (Corpus Callosum)

Adjusted for age, sex and TRS total score

Region	FA_Coef	FA_pval	MD_Coef	MD_pval
Corpus_Callosum_Body	-0.023	0.1913	0.060	0.2520
Corpus_Callosum_Combined	-0.019	0.3272	0.075	0.2324
Corpus_Callosum_Genu	-0.013	0.5328	0.083	0.3307
Corpus_Callosum_Splenium	-0.015	0.5579	0.079	0.3556

doi:10.6342/NTU202504209

Table 17.1 VBM Paired regression: early vs baseline, clustered by subject (Treated hand)

Adjusted for age, sex and TRS total score

Region	Coef	Pval_combined
L_preSMA	-0.005	0.8187
L_SMA	-0.016	0.5899
L_M1	-0.022	0.4650
L_VIM	-0.019	0.6062
L_VLp	-0.013	0.7182
R_Dorsal_Dentate_Nucleus	-0.005	0.5455
L_Red_Nucleus	0.002	0.2173
TRS	0.000	.

Region	Coef	Pval_combined
R_SCP	-0.003	0.9174
R_MCP	-0.008	0.6838
	-0.012	0.6092
R_ICP_HCP482		
R_ICP_JHU	-0.011	0.6858
TRS	0.000	.

doi:10.6342/NTU202504209

Table 17.2 VBM Paired regression: early vs baseline, clustered by subject (Non-treated hand)

Adjusted for age, sex and TRS total score

Region	Coef	Pval_combined
R_preSMA	-0.006	0.8041
R_SMA	0.019	0.6485
R_M1	0.007	0.8170
R_VIM	0.030	0.4445
R_VLp	0.022	0.5394
L_Dorsal_Dentate_Nucleus	-0.004	0.6967
R_Red_Nucleus	-0.004	0.0271*
TRS	0.000	.

Region	Coef	Pval_combined
L_SCP	-0.015	0.5836
L_MCP	-0.012	0.5507
L_ICP_HCP482	-0.024	0.2777
L_ICP_JHU	-0.010	0.6857
TRS	0.000	.

doi:10.6342/NTU202504209

Table 17.3 VBM Paired regression: early vs baseline, clustered by subject (Corpus callosum)

Adjusted for age, sex and TRS total score

Region	Coef	Pval_combined
Corpus_Callosum_Genu	0.022	0.5299
Corpus_Callosum_Body	0.017	0.5928
Corpus_Callosum_Splenium	0.022	0.5143
Corpus_Callosum_Combined	0.020	0.5352
TRS	0.000	.

doi:10.6342/NTU202504209

Table 18.1 Paired regression: DTI late vs baseline, clustered by subject (Treated hand)

Adjusted for age, sex and TRS total score

Region	FA_Coef	FA_pval	MD_Coef	MD_pval
L_Corticospinal_Tract	-0.004	0.8804	-0.035	1.0000
L_Frontopontine_Tract	0.002	0.8698	-0.054	1.0000
L_Medial_Lemniscus	-0.022	0.2257	0.016	1.0000
L_M1Vim	0.008	0.9573	-0.018	1.0000
L_VApreSMA_subject_mask	0.006	1.0000	-0.027	1.0000
L_VASMA_subject_mask	-0.005	0.8284	0.024	1.0000
R_SCP	0.005	0.8448	-0.060	0.8522
R_MCP	-0.022	0.2510	-0.004	0.8563
R_ICP_HCP482	-0.028	0.1674	0.004	0.9238
R_ICP_JHU	-0.037	0.0315*	0.024	0.9263

doi:10.6342/NTU202504209

Table 18.2 Paired regression: DTI late vs baseline, clustered by subject (Non-treated hand)

Adjusted for age, sex and TRS total score

Region	FA_Coef	FA_pval	MD_Coef	MD_pval
L_ICP_HCP482	0.002	1.0000	0.012	0.9420
L_ICP_JHU	-0.022	0.2876	0.020	1.0000
L_MCP	-0.012	1.0000	-0.001	0.9854
L_SCP	-0.023	1.0000	-0.023	0.9795
R_Corticospinal_Tract	0.008	1.0000	-0.054	1.0000
R_Frontopontine_Tract	-0.000	0.9581	-0.049	1.0000
R_M1Vim	-0.010	1.0000	-0.011	0.9837
R_Medial_Lemniscus	-0.016	1.0000	-0.004	1.0000
R_VASMA_subject_mask	-0.005	1.0000	-0.020	0.9666
R_VApreSMA_subject_mask	-0.017	1.0000	0.018	0.9082

doi:10.6342/NTU202504209

Table 18.3 Paired regression: DTI late vs baseline, clustered by subject (Corpus Callosum)

Adjusted for age, sex and TRS total score

Region	FA_Coef	FA_pval	MD_Coef	MD_pval
Corpus_Callosum_Body	0.006	0.8009	-0.040	0.3799
Corpus_Callosum_Combined	0.003	0.8733	-0.041	0.4298
Corpus_Callosum_Genu	-0.002	0.9298	-0.034	0.6228
Corpus_Callosum_Splenium	0.004	0.8090	-0.049	0.3132

doi:10.6342/NTU202504209

Table 19.1 VBM Paired regression: late vs baseline, clustered by subject (Treated hand)

Adjusted for age, sex and TRS total score

Region	Coef	Pval_combined
L_preSMA	-0.005	0.8729
L_SMA	0.011	0.7015
L_M1	-0.021	0.4768
L_VIM	0.079	0.2096
L_VLp	0.124	0.0610
R_Dorsal_Dentate_Nucleus	-0.007	0.3140
L_Red_Nucleus	-0.002	0.6161
TRS	0	.

Region	Coef	Pval_combined
R_SCP	-0.040	0.0911
R_MCP	-0.043	0.0256*
	-0.049	0.0240*
R_ICP_HCP 482		
R_ICP_JHU	-0.020	0.3938
TRS	0	.

doi:10.6342/NTU202504209

Table 19.2 VBM Paired regression: late vs baseline, clustered by subject (Non-treated hand)

Adjusted for age, sex and TRS total score

Region	Coef	Pval_combined
R_preSMA	0.006	0.8146
R_SMA	0.016	0.6828
R_M1	-0.040	0.1638
R_VIM	0.088	0.1320
R_VLp	0.098	0.0963
L_Dorsal_Dentate_Nucleus	-0.006	0.2653
R_Red_Nucleus	0.002	0.2636
TRS	0	.

Region	Coef	Pval_combined
L_SCP	-0.031	0.1225
L_MCP	-0.036	0.0606
L_ICP_HCP 482	-0.039	0.0750
L_ICP_JHU	-0.022	0.3231
TRS	0	.

doi:10.6342/NTU202504209

Table 19.3 VBM Paired regression: late vs baseline, clustered by subject (Corpus callosum)

Adjusted for age, sex and TRS total score

Region	Coef	Pval_combined
Corpus_Callosum_Genu	-0.012	0.4944
Corpus_Callosum_Body	0.003	0.7549
Corpus_Callosum_Spleniu m	-0.003	0.9337
Corpus_Callosum_Combine d	-0.003	0.8474
TRS	0	.

doi:10.6342/NTU202504209

Table 20.1 DTI ET vs. HC Summary

	Non-treated hand	Treated hand	Corpus callosum
ET v.s. HC			
ET-early v.s. HC	R_Frontopontine_Tract **(↑FA)**		Genu **(↑FA)** Body **(↑FA)** Splenium **(↑FA, ↓MD)** Combined **(↑FA)**
ET-late vs. HC	-	-	-

Table 20.2 DTI ET Longitudinal Comparison Summary

	Nontreated hand	Treated hand	Corpus callosum
ET-early vs. ET-baseline	-	-	-
ET-late vs. ET-baseline	-	R_ICP (JHU atlas) **(↓FA)** (Coef=-0.037, p = 0.0315*)	-

doi:10.6342/NTU202504209

Table 20.3 VBM ET vs. HC Summary

	Nondominant hand	Dominant hand	Corpus callosum
ET vs. HC	L_ICP (HCP482 atlas) (Coef = 0.105, p = 0.0244*)	R_MCP (Coef= 0.096, p = 0.0400*) R_ICP (HCP482 atlas) (Coef = 0.082, p = 0.0256*)	-

	Non treated hand	Treated hand	Corpus callosum
ET-early vs. HC	L_Dorsal_Dentate_Nucleus (Coef = 0.041, p = 0.0159)	R_Dorsal_Dentate_Nucleus (Coef= -0.035, p = 0.0252*)	-
ET-late vs. HC	-	-	-

Table 20.4 VBM ET Longitudinal Comparison Summary

	Nontreated hand	Treated hand	Corpus callosum
ET-early vs. ET-baseline	R_Red_Nucleus (Coef= -0.004, p = 0.0271*)	-	-
ET-late vs. ET-baseline	-	R_MCP (Coef= -0.043, p = 0.256*) R_ICP_HCP482 (Coef= -0.049, p = 0.0240*)	-

doi:10.6342/NTU202504209

Table 21.1 Cross-sectional regression of tremor severity metrics on onset_age, disease duration, and family history, adjusting for sex (with FDR)

	TRS	sel_Rt	sel_Lt
onset_age	0.545*	0.152**	0.111
	(0.237)	(0.048)	(0.084)
disease_duration	0.741	0.209*	0.206
	(0.359)	(0.073)	(0.127)
family_hx	5.489	1.184	1.598
	(9.315)	(1.884)	(3.289)
female	-11.454	-2.334	-3.189
	(7.668)	(1.551)	(2.707)
N	21	21	21

Standard errors in parentheses

* $p < 0.05$, ** $p < 0.01$, *** $p < 0.001$

doi:10.6342/NTU202504209

Table 21.2 Cross-Sectional Linear Regression of Baseline VBM on Total Tremor Rating Scale

Adjusted for age, sex and TRS total score

Cross-Sectional Linear Regression of Baseline VBM on Total Tremor Rating Scale (TRS)

ROI	coef	p	pval_fdr
R_Red_Nucleus	-1069.078	0.044*	0.609
L_VLp	37.067	0.078	0.544
R_M1	108.059	0.120	0.559
R_VLp	38.251	0.137	0.481
L_VIM	31.476	0.143	0.401
R_Dorsal_Dentate_Nucleus	-359.843	0.216	0.505
R_VIM	33.839	0.266	0.532
L_SMA	72.884	0.299	0.523
R_preSMA	-46.993	0.354	0.550
L_Dorsal_Dentate_Nucleus	-214.286	0.527	0.737
L_preSMA	-34.843	0.617	0.785
L_M1	33.168	0.735	0.857
R_SMA	-5.616	0.875	0.943
L_Red_Nucleus	34.914	0.954	0.954

*** $p < 0.001$, ** $p < 0.01$, * $p < 0.05$

Cross-Sectional Linear Regression of Baseline VBM on Total Tremor Rating Scale (TRS)

ROI	coef	p	pval_fdr
Corpus_Callosum_Genu	1.424	0.942	1
Corpus_Callosum_Body	3.954	0.867	1
Corpus_Callosum_Splenium	-5.117	0.871	1
Corpus_Callosum_Combined	0.027	0.999	0.999

doi:10.6342/NTU202504209

L_SCP	-43.510	0.477	1
R_SCP	-21.399	0.684	1
L_MCP	-63.843	0.298	1
R_MCP	-44.050	0.506	1
L_ICP_HCP482	-93.135	0.178	1
R_ICP_HCP482	-50.168	0.430	1
L_ICP_JHU	-40.834	0.506	1
R_ICP_JHU	-18.203	0.753	1

doi:10.6342/NTU202504209

Table 21.3 Cross-Sectional Linear Regression of Baseline VBM on Right-Hand Tremor Severity

Adjusted for age, sex and TRS total score

Cross-Sectional Linear Regression of Baseline VBM on Right-Hand Tremor Severity (sel_Rt)

ROI	coef	p	pval_fdr
R_Red_Nucleus	-172.539	0.053	0.743
L_VLp	7.983	0.069	0.484
L_SMA	15.844	0.120	0.562
R_VLp	7.712	0.124	0.435
R_Dorsal_Dentate_Nucleus	-69.034	0.126	0.354
L_Dorsal_Dentate_Nucleus	-93.810	0.143	0.335
L_VIM	5.577	0.231	0.463
R_VIM	4.773	0.424	0.741
L_preSMA	6.919	0.579	0.900
R_preSMA	-3.844	0.733	1
L_M1	-3.285	0.819	1
R_SMA	1.461	0.851	0.992
R_M1	-1.799	0.887	0.955
L_Red_Nucleus	12.911	0.911	0.911

Cross-Sectional Linear Regression of Baseline VBM on Right-Hand Tremor Severity (sel_Rt)

ROI	coef	p	pval_fdr
Corpus_Callosum_Genu	-4.850	0.329	0.438
Corpus_Callosum_Body	-2.599	0.556	0.607
Corpus_Callosum_Splenium	-0.686	0.895	0.895
Corpus_Callosum_Combined	-2.884	0.552	0.662
L_SCP	-14.629	0.179	0.307
R_SCP	-14.895	0.161	0.386
L_MCP	-21.724	0.066	0.398
R_MCP	-22.998	0.092	0.369

doi:10.6342/NTU202504209

L_ICP_HCP482	-25.630		0.561
		0.047*	
R_ICP_HCP482	-19.863	0.129	0.388
L_ICP_JHU	-17.147	0.166	0.332
R_ICP_JHU	-13.314	0.230	0.345

*** $p < 0.001$, ** $p < 0.01$, * $p < 0.05$

doi:10.6342/NTU202504209

Table 21.4 Cross-Sectional Linear Regression of Baseline VBM on Left-Hand Tremor Severity

Cross-Sectional Linear Regression of Baseline VBM on Left-Hand Tremor Severity (sel_Lt)

ROI	coef	p	pval_fdr
L_VLp	24.148	0.003**	0.046*
R_VLp	26.486	0.005**	0.038*
L_VIM	22.712	0.006**	0.026*
R_VIM	26.064	0.017*	0.059
R_Red_Nucleus	-315.325	0.168	0.469
R_Dorsal_Dentate_Nucleus	-111.102	0.237	0.553
R_M1	30.086	0.299	0.598
L_M1	22.232	0.484	0.847
L_Red_Nucleus	-131.699	0.543	0.844
L_SMA	17.054	0.568	0.796
L_Dorsal_Dentate_Nucleus	-63.743	0.620	0.789
R_preSMA	-10.263	0.624	0.728
L_preSMA	0.598	0.981	1
R_SMA	0.083	0.996	0.996

Cross-Sectional Linear Regression of Baseline VBM on Left-Hand Tremor Severity (sel_Lt)

ROI	coef	p	pval_fdr
Corpus_Callosum_Genu	-6.136	0.416	0.625
Corpus_Callosum_Body	-3.807	0.666	0.727
Corpus_Callosum_Splenium	-3.990	0.753	0.753
Corpus_Callosum_Combined	-5.014	0.603	0.724
L_SCP	-23.501	0.208	0.499

doi:10.6342/NTU202504209

R_SCP	-16.099	0.318	0.636
L_MCP	-38.390		0.231
		0.039*	
R_MCP	-30.553	0.103	0.414
L_ICP_HCP482	-43.640		0.320
		0.027*	
R_ICP_HCP482	-23.004	0.133	0.399
L_ICP_JHU	-16.429	0.383	0.657
R_ICP_JHU	-12.286	0.535	0.713

doi:10.6342/NTU202504209

Table 21.5 Cross-Sectional Linear Regression of Baseline DTI Scalar Indices on TRS total score

Adjusted for age, sex and TRS total score

outcome	scalar_kind	roi	pval	pval_fdr
TRS	FA	Corpus_Callosum_Genu	0.981	1
TRS	FA	Corpus_Callosum_Body	0.845	1
TRS	FA	Corpus_Callosum_Splenium	0.962	1
TRS	FA	Corpus_Callosum_Combined	0.969	1
TRS	FA	L_Corticospinal_Tract	0.092	0.811
TRS	FA	L_Medial_Lemniscus	0.884	1
TRS	FA	L_Frontopontine_Tract	0.303	1
TRS	FA	L_M1_Vim	.	1
TRS	FA	R_Corticospinal_Tract	0.075	0.828
TRS	FA	R_Medial_Lemniscus	0.993	1
TRS	FA	R_Frontopontine_Tract	0.174	0.849
TRS	FA	R_M1_Vim	.	1
TRS	FA	L_SCP	0.602	1
TRS	FA	L_MCP	0.627	1
TRS	FA	L_ICP_HCP482	0.859	1
TRS	FA	L_ICP_JHU	0.559	1
TRS	FA	R_SCP	0.537	1
TRS	FA	R_MCP	0.365	1
TRS	FA	R_ICP_HCP482	0.285	1
TRS	FA	R_ICP_JHU		1

doi:10.6342/NTU202504209

			0.443	
TRS	MD	Corpus_Callosum_Genu	0.880	1
TRS	MD	Corpus_Callosum_Body	0.194	0.854
TRS	MD	Corpus_Callosum_Splenium	0.334	1
TRS	MD	Corpus_Callosum_Combined	0.372	1
TRS	MD	L_Corticospinal_Tract	0.901	1
TRS	MD	L_Medial_Lemniscus	0.851	1
TRS	MD	L_Frontopontine_Tract	0.482	1
TRS	MD	L_M1_Vim	0.842	1
TRS	MD	R_Corticospinal_Tract	0.475	1
TRS	MD	R_Medial_Lemniscus	0.347	1
TRS	MD	R_Frontopontine_Tract	0.393	1
TRS	MD	R_M1_Vim	0.840	1
TRS	MD	L_SCP	0.099	0.724
TRS	MD	L_MCP	0.722	1
TRS	MD	L_ICP_HCP482	0.146	0.801
TRS	MD	L_ICP_JHU	0.815	1
TRS	MD	R_SCP	0.605	1
TRS	MD	R_MCP	0.795	1
TRS	MD	R_ICP_HCP482	0.117	0.733
TRS	MD	R_ICP_JHU	0.008 **	0.344
TRS	MD	R_M1Vim	.	1
TRS	FA	L_M1Vim	0.008 **	0.179

doi:10.6342/NTU202504209

TRS	MD	L_M1Vim	.	1
TRS	FA	R_M1Vim		1
			0.070	

*** $p < 0.001$, ** $p < 0.01$, * $p < 0.05$

doi:10.6342/NTU202504209

Table 21.6 Cross-Sectional Linear Regression of Baseline DTI Scalar Indices on sum of TRS selected items (Right Hand)

Adjusted for age, sex and TRS total score

outcome	scalar_kind	roi	pval	pval_fdr
sel_Rt	FA	Corpus_Callosum_Genu	0.159	0.412
sel_Rt	FA	Corpus_Callosum_Body	0.186	0.454
sel_Rt	FA	Corpus_Callosum_Splenium	0.259	0.569
sel_Rt	FA	Corpus_Callosum_Combined	0.122	0.384
sel_Rt	FA	L_Corticospinal_Tract	0.019*	0.209
sel_Rt	FA	L_Medial_Lemniscus	0.560	0.795
sel_Rt	FA	L_Frontopontine_Tract	0.355	0.624
sel_Rt	FA	L_M1_Vim	.	1
sel_Rt	FA	R_Corticospinal_Tract	0.095	0.322
sel_Rt	FA	R_Medial_Lemniscus	0.489	0.768
sel_Rt	FA	R_Frontopontine_Tract	0.013*	0.284
sel_Rt	FA	R_M1_Vim	.	1
sel_Rt	FA	L_SCP	0.963	1
sel_Rt	FA	L_MCP	0.567	0.780
sel_Rt	FA	L_ICP_HCP482	0.532	0.808
sel_Rt	FA	L_ICP_JHU	0.939	1
sel_Rt	FA	R_SCP	0.271	0.568
sel_Rt	FA	R_MCP	0.091	0.334
sel_Rt	FA	R_ICP_HCP482	0.663	0.858
sel_Rt	FA	R_ICP_JHU	0.316	0.604
sel_Rt	MD	Corpus_Callosum_Genu	0.149	0.411
sel_Rt	MD	Corpus_Callosum_Body	0.777	0.976
sel_Rt	MD	Corpus_Callosum_Splenium	0.899	1
sel_Rt	MD	Corpus_Callosum_Combined	0.550	0.807
sel_Rt	MD	L_Corticospinal_Tract	0.068	0.300
sel_Rt	MD	L_Medial_Lemniscus	0.444	0.751
sel_Rt	MD	L_Frontopontine_Tract	0.064	0.349
sel_Rt	MD	L_M1_Vim	0.063	0.398
sel_Rt	MD	R_Corticospinal_Tract	0.031*	0.276

doi:10.6342/NTU202504209

sel_Rt	MD	R_Medial_Lemniscus	0.309	0.619
sel_Rt	MD	R_Frontopontine_Tract	0.015*	0.219
sel_Rt	MD	R_M1_Vim	0.067	0.327
sel_Rt	MD	L_SCP	0.835	1
sel_Rt	MD	L_MCP	0.136	0.398
sel_Rt	MD	L_ICP_HCP482	0.860	1
sel_Rt	MD	L_ICP_JHU	0.323	0.592
sel_Rt	MD	R_SCP	0.256	0.592
sel_Rt	MD	R_MCP	0.080	0.321
sel_Rt	MD	R_ICP_HCP482	0.589	0.786
sel_Rt	MD	R_ICP_JHU	0.448	0.730
sel_Rt	MD	R_M1Vim	.	1
sel_Rt	FA	L_M1Vim	0.004**	0.155
sel_Rt	FA	R_M1Vim	0.052	0.382
sel_Rt	MD	L_M1Vim	.	1

*** $p < 0.001$, ** $p < 0.01$, * $p < 0.05$

doi:10.6342/NTU202504209

Table 21.7 Cross-Sectional Linear Regression of Baseline DTI Scalar Indices on sum of TRS selected items (Left Hand)

outcome	scalar_kind	roi	pval	pval_fdr
sel_Lt	FA	Corpus_Callosum_Genu	0.478	1
sel_Lt	FA	Corpus_Callosum_Body	0.493	0.987
sel_Lt	FA	Corpus_Callosum_Splenium	0.720	1
sel_Lt	FA	Corpus_Callosum_Combined	0.550	1
sel_Lt	FA	L_Corticospinal_Tract	0.044*	0.483
sel_Lt	FA	L_Medial_Lemniscus	0.595	0.969
sel_Lt	FA	L_Frontopontine_Tract	0.332	0.914
sel_Lt	FA	L_M1_Vim	.	1
sel_Lt	FA	R_Corticospinal_Tract	0.207	1
sel_Lt	FA	R_Medial_Lemniscus	0.735	1
sel_Lt	FA	R_Frontopontine_Tract	0.427	0.939
sel_Lt	FA	R_M1_Vim	.	1
sel_Lt	FA	L_SCP	0.844	1
sel_Lt	FA	L_MCP	0.803	1
sel_Lt	FA	L_ICP_HCP482	0.742	1
sel_Lt	FA	L_ICP_JHU	0.349	0.854
sel_Lt	FA	R_SCP	0.595	0.935
sel_Lt	FA	R_MCP	0.524	1
sel_Lt	FA	R_ICP_HCP482	0.169	1
sel_Lt	FA	R_ICP_JHU	0.336	0.870
sel_Lt	MD	Corpus_Callosum_Genu		

doi:10.6342/NTU202504209

			0.626	0.950
sel_Lt	MD	Corpus_Callosum_Body		1
			0.326	
sel_Lt	MD	Corpus_Callosum_Splenium		1
			0.280	
sel_Lt	MD	Corpus_Callosum_Combined		1
			0.317	
sel_Lt	MD	L_Corticospinal_Tract		
			0.572	0.968
sel_Lt	MD	L_Medial_Lemniscus		1
			0.919	
sel_Lt	MD	L_Frontopontine_Tract		1
			0.266	
sel_Lt	MD	L_M1_Vim		
			0.874	0.986
sel_Lt	MD	R_Corticospinal_Tract		1
			0.303	
sel_Lt	MD	R_Medial_Lemniscus		
			0.384	0.889
sel_Lt	MD	R_Frontopontine_Tract		1
			0.202	
sel_Lt	MD	R_M1_Vim		1
			0.848	
sel_Lt	MD	L_SCP		
			0.327	0.960
sel_Lt	MD	L_MCP		1
			0.837	
sel_Lt	MD	L_ICP_HCP482		1
			0.291	
sel_Lt	MD	L_ICP_JHU		
			0.556	0.979
sel_Lt	MD	R_SCP		1
			0.836	
sel_Lt	MD	R_MCP		
			0.849	0.983
sel_Lt	MD	R_ICP_HCP482		1
			0.158	
sel_Lt	MD	R_ICP_JHU		
			0.016*	0.346
sel_Lt	MD	R_M1Vim	.	1
sel_Lt	FA	L_M1Vim		
			0.014*	0.616
sel_Lt	MD	L_M1Vim	.	1
sel_Lt	FA	R_M1Vim		
			0.026*	0.378

doi:10.6342/NTU202504209

Table 22.1 Multiple Linear Regression: Clinical Predictors of Improvement (TRS, sel_Rt, sel_Lt) with FDR

	TRS_%improved	sel_Rt%improved	sel_Lt%improved
Age at time of treatment	0.720*	0.359	-0.295
	(0.358)	(0.552)	(0.834)
Baseline TRS	-0.612*	-0.154	-0.062
	(0.293)	(0.448)	(0.724)
Baseline sel_Rt	0.988	-1.731	2.625
	(1.825)	(2.789)	(4.483)
Skull density ratio (SDR)	4.937	56.561	13.443
	(37.501)	(57.834)	(88.257)
Family history (1=yes)	24.461*	24.274	45.750
	(12.409)	(19.252)	(28.115)
Sex (Female=1)	8.350	20.344	18.526
	(11.014)	(17.015)	(25.729)
Time interval between treatment and TRS evaluation (months)	-0.450**	-0.379	-0.870***
	(0.158)	(0.256)	(0.195)
Observations	20	20	20

All models use random intercept for subject; REML estimation.

* $p < 0.05$, ** $p < 0.01$, *** $p < 0.001$

doi:10.6342/NTU202504209

Table 22.2 Multiple Linear Regression: Clinical Predictors of Improvement (TRS, sel_Rt, sel_Lt)

	TRS_%improved	sel_Rt%improved	sel_Lt%improved
Age at time of treatment	1.045**	0.438	0.687
	(0.372)	(0.419)	(0.804)
baseline_TRS	-0.306	-0.189	0.382
	(0.371)	(0.412)	(0.810)
Sex (Female=1)	9.402	11.023	11.834
	(13.735)	(15.534)	(29.654)
Time interval between treatment and TRS evaluation (months)	-0.450**	-0.482	-0.864***
	(0.174)	(0.262)	(0.199)
Max Energy (J)	-0.000	-0.001	0.000
	(0.001)	(0.001)	(0.001)
Max Watt (W)	0.019	0.048	0.021
	(0.041)	(0.045)	(0.090)
Max Temp (℃)	1.097	-3.290	-0.417
	(3.315)	(3.670)	(7.269)
Sonications	-3.928	-1.368	-10.040
	(4.453)	(5.151)	(9.432)
>50℃ Sonications	3.368	8.071	10.946
	(9.496)	(10.548)	(20.766)
Observations	20	20	20

All models use random intercept for subject_id; REML estimation. * $p < 0.05$, ** $p < 0.01$, *** $p < 0.001$

doi:10.6342/NTU202504209

Table 22.3 Baseline VBM Predictors of TRS Improvement

FDR-corrected, adjusted for age, sex, time interval between treatment and TRS evaluation, baseline TRS

ROI	coef	se	pval	Significance	pval_fdr	Significance_FDR
L_preSMA	-124.888	66.954	0.083		0.291	.
R_preSMA	-109.983	56.066	0.070		0.327	.
L_SMA	51.334	54.811	0.365		0.730	.
R_SMA	-2.515	42.948	0.954		1	.
L_M1	-16.412	74.927	0.830		1	.
R_M1	-203.532	71.805	0.013	*	0.185	.
L_VIM	1.057	43.667	0.981		0.981	.
R_VIM	1.286	52.417	0.981		1	.
L_VLp	8.316	45.805	0.859		1	.
R_VLp	17.791	56.493	0.757		1	.
L_Dorsal_Dentate_Nucleus	65.092	329.002	0.846		1	.
R_Dorsal_Dentate_Nucleus	-248.452	230.592	0.299		0.699	.
L_Red_Nucleus	-1302.795	571.050	0.039	*	0.271	.
R_Red_Nucleus	-1180.891	856.779	0.190		0.531	.

* $p < 0.05$, ** $p < 0.01$, *** $p < 0.001$

doi:10.6342/NTU202504209

ROI	coef	se	pval	Significance	pval_fdr	Significance_FDR
Corpus_Callosum_Genu	-62.597	53.054	0.258	.	0.773	.
Corpus_Callosum_Body	-75.896	58.223	0.213	.	0.854	.
Corpus_Callosum_Splenium	-71.090	49.614	0.174	.	1	.
Corpus_Callosum_Combined	-78.402	56.023	0.183	.	1	.
L_SCP	11.969	64.536	0.856	.	1	.
R_SCP	7.705	66.147	0.909	.	0.992	.
L_MCP	-13.783	88.217	0.878	.	1	.
R_MCP	-10.216	87.857	0.909	.	0.909	.
L_ICP_HCP482	15.701	76.565	0.840	.	1	.
R_ICP_HCP482	11.186	75.364	0.884	.	1	.
L_ICP_JHU	19.132	67.266	0.780	.	1	.
R_ICP_JHU	24.740	60.259	0.688	.	1	.

doi:10.6342/NTU202504209

Table 22.4 Baseline VBM Predictors of Treated Hand Improvement

FDR-corrected, adjusted for age, sex, time interval between treatment and TRS evaluation, baseline TRS

ROI	coef	se	pval	Significance	pval_fdr	Significance_FDR
L_preSMA	-18.215	107.154	0.867	.	1	.
R_preSMA	-34.671	90.290	0.707	.	1	.
L_SMA	2.650	81.009	0.974	.	1	.
R_SMA	-40.411	60.631	0.516	.	1	.
L_M1	168.475	97.741	0.107	.	0.498	.
R_M1	-206.557	116.767	0.099	.	0.691	.
L_VIM	11.858	62.530	0.852	.	1	.
R_VIM	-30.479	74.713	0.689	.	1	.
L_VLp	11.939	65.674	0.858	.	1	.
R_VLp	-21.582	81.079	0.794	.	1	.
L_Dorsal_Dentate_Nucleus	830.782	416.940	0.066	.	0.926	.
R_Dorsal_Dentate_Nucleus	37.596	343.907	0.915	.	1	.
L_Red_Nucleus	-2.940	958.954	0.998	.	0.998	.
R_Red_Nucleus	-50.725	1309.057	0.970	.	1	.

doi:10.6342/NTU202504209

ROI	coef	se	pval	Significance	pval_fdr	Significance_FDR
Corpus_Callosum_Genu	-97.849	75.351	0.215		0.645	.
Corpus_Callosum_Body	-118.011	82.583	0.175		0.700	.
Corpus_Callosum_Splenium	-168.230	61.488	0.016	*	0.193	.
Corpus_Callosum_Combined	-148.434	76.033	0.071		0.427	.
L_SCP	-11.965	92.589	0.899		1	.
R_SCP	-3.180	94.882	0.974		0.974	.
L_MCP	49.385	125.903	0.701		1	.
R_MCP	12.428	125.984	0.923		1	.
L_ICP_HCP482	10.741	109.905	0.924		1	.
R_ICP_HCP482	52.639	107.221	0.631		1	.
L_ICP_JHU	6.672	96.707	0.946		1	.
R_ICP_JHU	-3.570	86.911	0.968		1	.

doi:10.6342/NTU202504209

Table 22.5 Baseline VBM Predictors of Non-treated Hand Improvement

FDR-corrected, adjusted for age, sex, time interval between treatment and TRS evaluation, baseline TRS

ROI	coef	se	pval	Significance	pval_fdr	Significance_FDR
L_preSMA	-128.756	155.884	0.423		0.986	.
R_preSMA	-166.699	127.521	0.212		1	.
L_SMA	-69.895	119.110	0.567		0.793	.
R_SMA	-80.843	89.072	0.379		1	.
L_M1	-139.237	155.772	0.387		1	.
R_M1	-100.684	190.328	0.605		0.652	.
L_VIM	54.220	92.046	0.565		0.879	.
R_VIM	49.939	111.051	0.660		0.660	.
L_VLp	52.899	96.828	0.593		0.755	.
R_VLp	94.822	118.287	0.436		0.872	.
L_Dorsal_Dentate_Nucleus	850.812	665.222	0.222		1	.
R_Dorsal_Dentate_Nucleus	275.852	506.702	0.595		0.694	.
L_Red_Nucleus	-3364.836	1108.182	0.009	**	0.124	.
R_Red_Nucleus	-1363.180	1913.939	0.488		0.854	.

doi:10.6342/NTU202504209

ROI	coef	se	pval	Significance	pval_fdr	Significance_FDR
Corpus_Callosum_Genu	-38.469	118.257	0.750	.	1	.
Corpus_Callosum_Body	-45.720	130.993	0.732	.	1	.
Corpus_Callosum_Splenium	30.119	113.078	0.794	.	1	.
Corpus_Callosum_Combined	-14.101	127.576	0.914	.	0.914	.
L_SCP	49.705	137.236	0.723	.	1	.
R_SCP	56.337	140.409	0.694	.	1	.
L_MCP	-151.509	183.999	0.424	.	1	.
R_MCP	-22.800	187.462	0.905	.	0.987	.
L_ICP_HCP482	-69.782	162.555	0.674	.	1	.
R_ICP_HCP482	-38.845	160.604	0.812	.	1	.
L_ICP_JHU	26.548	143.773	0.856	.	1	.
R_ICP_JHU	55.194	128.509	0.674	.	1	.

doi:10.6342/NTU202504209

Table 23.1 Summary of Clinical Predictors of Improvement of Tremor in the treated hand (sel_Rt)

Correlation with tremor improvement (%)	Factors
Positive ($\beta > 0$, $p < 0.05$)	Older age at treatment
Negative ($\beta < 0$, $p < 0.05$)	Older age of onset
Neutral Effect ($p \geq 0.05$)	- Disease duration - Baseline TRS - Baseline severity of right hand tremor (sel_Rt) - SDR - Family history - All treatment parameters examined - VBM value of all ROIs (gray matter, white matter) examined

doi:10.6342/NTU202504209

Table 23.2 Summary of Clinical Predictors of Improvement of Tremor in the nontreated hand (sel_Lt)

Correlation with tremor improvement (%)	Factors
Positive ($\beta > 0$, $p < 0.05$)	- Older age at treatment - Family history of tremor
Negative ($\beta < 0$, $p < 0.05$)	- Older age of onset - Longer disease duration - Longer time interval at the time of observation
Neutral Effect ($p \geq 0.05$)	- Baseline TRS - Baseline severity of right hand tremor (sel_Rt) - SDR - All treatment parameters examined - VBM value of all ROIs (gray matter, white matter) examined

doi:10.6342/NTU202504209

Table 24.1 Mixed Model: Clinical Predictors of Improvement in TRS part C with FDR

	TRS C % improved
Age at time of treatment	1.790**
	(0.560)
Baseline TRS	-0.230
	(0.410)
Baseline sel_Rt	-1.092
	(2.584)
Skull density ratio (SDR)	-79.326
	(58.503)
Family history (1=yes)	35.841
	(20.188)
Sex (Female=1)	-16.333
	(17.515)
Time interval between treatment and TRS evaluation (months)	-0.345
	(0.326)
Observations	20

All models use random intercept for subject; REML estimation. Raw p-values shown. FDR-adjusted p-values exported separately.
* $p < 0.05$, ** $p < 0.01$, *** $p < 0.001$

doi:10.6342/NTU202504209

Table 24.2 Mixed Model: Clinical Predictors of Improvement in TRS part A+B with FDR

	TRS A+B % improved
Age at time of treatment	0.295
	(0.452)
Baseline TRS	-0.647
	(0.394)
Baseline sel_Rt	1.230
	(2.435)
Skull density ratio (SDR)	26.510
	(47.866)
Family history (1=yes)	20.167
	(15.222)
Sex (Female=1)	15.387
	(13.951)
Time interval between treatment and TRS evaluation (months)	-0.332***
	(0.100)
Observations	20

All models use random intercept for subject; REML estimation. Raw p-values shown. FDR-adjusted p-values exported separately.
* $p < 0.05$, ** $p < 0.01$, *** $p < 0.001$

doi:10.6342/NTU202504209